Metallurgical Processing and Superconducting Parameters of the V_3Ga A15 Phase

B. N. DAS AND J. E. COX
Material Sciences Division

and

R. W. HUBER
Electronics Technology Division

September 10, 1975

NAVAL RESEARCH LABORATORY
Washington, D.C.

REPORT DOCUMENTATION PAGE

READ INSTRUCTIONS BEFORE COMPLETING FORM

1. REPORT NUMBER: NRL Report 7907
2. GOVT ACCESSION NO.:
3. RECIPIENT'S CATALOG NUMBER:

4. TITLE (and Subtitle): METALLURGICAL PROCESSING AND SUPERCONDUCTING PARAMETERS OF THE V_3Ga A15 PHASE

5. TYPE OF REPORT & PERIOD COVERED: Final report on one phase of a continuing NRL problem.

6. PERFORMING ORG. REPORT NUMBER:

7. AUTHOR(s): B. N. Das, R. W. Huber, and J. E. Cox

8. CONTRACT OR GRANT NUMBER(s):

9. PERFORMING ORGANIZATION NAME AND ADDRESS: Naval Research Laboratory, Washington, D. C. 20375

10. PROGRAM ELEMENT, PROJECT, TASK AREA & WORK UNIT NUMBERS: NRL Problem M01-09, Project RR022-01-46-5407

11. CONTROLLING OFFICE NAME AND ADDRESS: Office of Naval Research, Arlington, Va. 22217

12. REPORT DATE: September 10, 1975

13. NUMBER OF PAGES: 45

14. MONITORING AGENCY NAME & ADDRESS (if different from Controlling Office):

15. SECURITY CLASS. (of this report): UNCLASSIFIED

15a. DECLASSIFICATION/DOWNGRADING SCHEDULE:

16. DISTRIBUTION STATEMENT (of this Report)

Approved for public release; distribution unlimited.

17. DISTRIBUTION STATEMENT (of the abstract entered in Block 20, if different from Report)

18. SUPPLEMENTARY NOTES

19. KEY WORDS (Continue on reverse side if necessary and identify by block number)

Superconductivity
A15 (V_3Ga)
Microstructure
Microhardness
Lattice parameter
Long-range order

20. ABSTRACT (Continue on reverse side if necessary and identify by block number)

The solid-state bcc-to-A15 phase transformation in V_3Ga, the extension of this A15 phase field on both sides of the stoichiometric composition, and the high-field current-carrying capacity of V_3Ga composite wires make V_3Ga attractive for investigating how structure determines superconducting properties. However the extended freezing range in the V-Ga binary system promotes both dendritic segregation and a large-scale radial Ga gradient. For systematic study of the interrelations among the metallurgical processing procedures, the resultant microstructures, and the superconducting properties of the V_3Ga A15 phase, eleven alloys, spanning the composition range of the A15 phase field and the adjacent two-phase fields, were arc-melted and cast as 1.3 cm-diameter rods.

UNCLASSIFIED

The dendritic segregation in the cast materials was made visible in metallographic sections by etching. A brief heat treatment at temperatures in the bcc-phase field eliminates the dendritic segregation and reduces the radial Ga gradient. By rapidly cooling the specimen through the bcc-to-A15 transformation, segregation from the transformation is on a fine scale and can be removed by a subsequent anneal within the β-phase field. The transformed microstructures and the annealed microstructures of all materials of the V_3Ga A15 phase were similar, and even microhardness was nearly constant over the full broad composition range of the V_3Ga phase. The lattice parameter of the A15 V_3Ga phase, measured by powder x-ray diffraction, increased with increasing Ga content. The present measurements define two lines intersecting near the V_3Ga composition. These data suggest that the composition adjusts by substitution of V and Ga atoms in V_3Ga. The long-range-order studies showed that the A15 V_3Ga phase is highly ordered, even in the cast state. The superconducting transition temperature, T_0, drops rapidly from a maximum as the composition deviates from stoichiometry. Measured values of T_0 without accompanying critical-magnetic-field information can be up to several tenths of a kelvin too high. Several superconducting parameters for the homogeneous V_3Ga phase are evaluated from the slope of the critical-magnetic-field curves. Analysis of the initial slope of the critical-magnetic-field-vs-composition plot and of the transition-temperature-vs-composition plot suggest that on the Ga-rich side of the stoichiometry the Labbé-Friedel linear chain model holds but that on the V-rich side the density-of-states model seems more valid.

CONTENTS

METALLURGICAL PROCESSING AND SUPERCONDUCTING PARAMETERS OF THE V_3Ga A15 PHASE

INTRODUCTION

For a variety of superconducting applications, materials are required with high critical temperatures, magnetic fields, and currents. Many intermetallic phases of several structural types (A15, Laves, sigma, and sodium chloride) as well as bcc metals and alloys (Nb, Nb-Ti, and Nb-Zr) qualify as high-field superconductors. Among these materials however intermediate phases with the A15 structure possess the highest superconducting transition temperatures T_0, determined to date. Of the several high-field binary and ternary A15 materials (including Nb_3Al, Nb_3Ga, Nb_3Sn, V_3Si, and $Nb_3Al_{.75}Ge_{.25}$), V_3Ga is particularly attractive both as a practical superconductor and as a research material for investigating the role of structure in determining the superconducting properties. The advantages of the V_3Ga phase in studying how structure affects properties derive from the nature of the phase equilibria in the V-Ga system (Fig. 1). [1]

The A15 phase of the V-Ga system is a superconductor with demonstrated technological potential. Recently at the Naval Research Laboratory V_3Ga formed in composite wires achieved the highest critical current density (10^6 A/cm^2) measured at 100 kG [2]. Other A15 phases with "superior" superconducting properties are ranked in Table 1. Most of the values listed there are for laboratory specimens, since only Nb_3Sn and, very recently, V_3Ga have been developed as superconducting materials of commercial interest. For all of these materials the superconducting properties are highly dependent on the composition of the A15 phase—generally attaining their optimum values near the stoichiometric A_3B composition.

The stoichiometric Nb_3Ge and Nb_3Ga A15 phases do not exist in the equilibrium state, and stoichiometric Nb_3Al is unstable below 1600°C; the data shown in Table 1 for these materials are from small quenched specimens or unstable thin films. Since these structures are metastable, it is difficult to achieve meaningful structural modification through processing (or even to evaluate the existing structure fully). The addition of Ge to Nb_3Al stabilizes the stoichiometric A15 structure as $Nb_3(Al_{.75}Ge_{.25})$. However the phase equilibria of this ternary system are only partially defined; thus the potential for structural manipulations cannot be evaluated. Both Nb-Sn and V-Si are systems in which the stoichiometric A_3B composition nearly coincides with the high B-element limit of the A15 phase field. This circumstance does not detract from the usefulness of these materials (the wide use of Nb_3Sn in high-field magnets is evidence of this) but does impose a compositional restriction that would impair study of the structure-and-property interrelations.

On the other hand, V-Ga is a system in which the broad compositional range of the A15 phase spans the stoichiometric V_3Ga composition. The phase equilibria of this

Note: Manuscript submitted May 2, 1975.

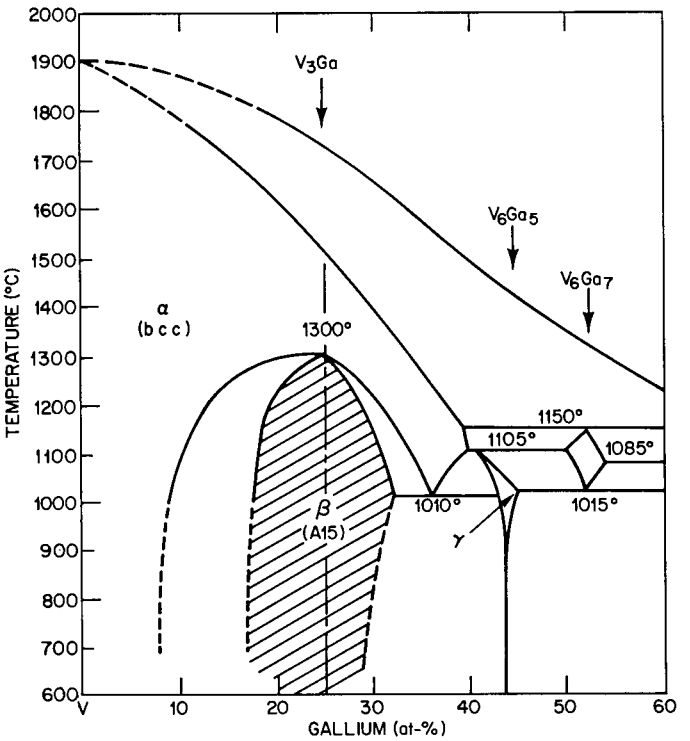

Fig. 1—Vanadium-gallium phase diagram as reported by van Vucht et al. [1]

Table 1
Superconducting Properties of A15 Phases

Materials	Transition Temperature T_0 (K)	Critical Field H_{c2} at 4.2 K (kOe)	Critical Current Density J_c at 100 kOe and 4.2 K (10^4 A/cm^2)
Nb_3Ge	22.5	—	—
$Nb_3(Al_3Ge)$	20.5	410	0.3
Nb_3Ga	20.3	340	3
Nb_3Al	18.8	295	50
Nb_3Sn	18.0	225	5-30
V_3Si	17.1	230	5
V_3Ga	15.3	220	100

system, defined principally by the work of van Vucht et al. [1] and presented in part in Fig. 1, have a number of interesting aspects which may be used in processing the superconducting material and modifying its microstructure. At high temperature the A15 phase is in equilibrium with the bcc phase. This bcc-to-A15 transformation may provide a means for refining the grain structure of the superconductor. The precipitation of V_6Ga_5 within Ga-rich A15, indicated by the decreasing solubility limit of the A15 phase, may provide flux-pinning centers in the superconductor. These properties of the V-Ga system suggest that, by controlled processing, a variety of materials of different compositions and structures can be produced and the influence of these structural variables on the superconducting properties can be evaluated.

The phase diagram also indicates one difficulty in preparing homogeneous specimens of the superconducting phase. The extended freezing range for the compositions of the A15 phase will lead to pronounced dendritic segregation in cast materials. Accordingly cast materials must be homogenized to eliminate this solidification segregation. The bcc solid-solution phase field that exists at temperatures above the A15 stability range provides a means for accelerating this homogenization. That is, by annealing a casting at high temperature in the bcc condition (where diffusion is fast), by rapidly cooling to generate a fine A15 structure through the transformation, and finally by annealing in the A15 stability range to remove the fine-scale transformation segregation, this problem may be eliminated.

This report gives the results of a systematic study of the interrelations among the metallurgical processing, the resultant microstructures, and the superconducting properties of the V-Ga A15 phase. Eleven alloys, spanning the entire composition range of the A15 field and the adjacent two-phase fields, were arc-melted and cast as 1.3-cm-diameter rods. The structures of these rods were examined, and the effects of high-temperature homogenization, transformation, and annealing on the microstructure and on the lattice parameter of the A15 phase were evaluated by metallographic, x-ray-diffraction, and microhardness measurements. The long-range-order parameter has been evaluated for three compositions near the stoichiometric V_3Ga in each of the three processing conditions: cast, transformed, and annealed. The superconducting properties of a series of transformed and annealed specimens were measured and related to composition, structure, and long-range order.

TERMINOLOGY, DEFINITIONS, AND LIMITS OF ACCURACY

Throughout the remainder of this report the phase designations of Fig. 1 will be used: α is the terminal bcc solid solution, β is the A15 phase, which includes the stoichiometric V_3Ga composition, and γ is the hexagonal phase (Ti_6Sn_5 type), most frequently indicated as V_6Ga_5.

Although a variety of heat-treating procedures were used to evaluate phase equilibria and long-range-order parameters, the specimens for the major part of the study were in three distinct metallurgical states:

Cast. The arc-cast material is characterized by distinct dendritic segregation originating in the solidification process.

Transformed. Cast material heat-treated in the α state to eliminate the solidification segregation and rapidly cooled through the α-to-β transformation is characterized by a relatively fine β-phase grain size and by microsegregation generated in the α-to-β transformation.

Annealed. Transformed material annealed in the β state to eliminate the micro segregation from the α-to-β transformation is characterized by a homogeneous β phase of a larger grain size than that of the transformed specimen.

All specimen compositions are given in atomic percent, and an abbreviated specimen notation is used. Thus, V-13.3Ga is used in place of the cumbersome 86.7 at-% V, 13.3 at-% Ga. The V content of each cast rod was determined by chemical analysis, with an accuracy of ±0.5 wt-%. The Ga content, determined by difference, has been converted to atomic percent. However in presenting these analyses and the impurity concentrations we will retain the weight-percent usage of the analyst.

All processing temperatures are reported in degrees Celsius (°C). The temperature of the induction annealing furnace was measured to an accuracy of ±5°C, and the temperatures of the tubular resistance furnaces, used for annealing samples between 700 and 800°C, were measured to ±1°C. The temperatures of the cryogenic experiments are reported in kelvins (K). The accuracy of the cryogenic measurements are within ±30 millikelvins.

For all x-ray diffraction work, we used Cu radiation (K_{a1} = 1.54051 Å, K_{a2} = 1.54433 Å, and K_a = 1.54178 Å). The lattice parameters were evaluated from the powder patterns (114.6-mm-diameter cameras with a Straumanis film-loading arrangement), and use of the Nelson-Riley extrapolation function provided an accuracy of ±0.0005 Å.

EXPERIMENTAL PROCEDURES:

Arc-Melting and Casting

To prepare the V-Ga specimens, the pure metals were weighed, mixed, and compacted into briquets at 1500 kg/cm^2. The electrolytic V was of a coarse (1 to 12 mm), irregular, dendritic form. The Ga was chilled in liquid nitrogen and crushed to <10 mesh particles in a hardened steel mortar. The briquets, weighing approximately 100 g, were melted in an arc furnace (water-cooled tungsten electrode and copper hearth) using dc currents of 300 A. The atmosphere was 99.995% pure argon, and this gas was first passed through heated Ti and Zr turnings to remove nitrogen and oxygen, and then through a cold trap to condense any trace of water vapor. The specimens were inverted on the copper hearth and remelted four times to achieve complete alloying between the V and Ga.

The need for a number of samples of identical composition for the individual experiments of this study necessitated large (100-g) button melts. Also this investigation required specimens of uniform and similar, if not identical, microstructure. In arc-melting such large specimens on a water-cooled copper hearth, the entire specimen cannot be maintained in the liquid state. Thus the highly directional solidification

pattern, pronounced in small button melts, is made much more complex, and the microstructure of the resulting button varies from the fine-grained structure of a chill zone, to cellular, to rather coarse dendritic. To obtain a more uniform structure, these buttons were remelted and cast as rods.

For the casting process the button was arc-melted on a copper hearth machined into the top of a heavy-walled split copper mold. The surface of the button was rapidly melted and, by increasing the arc current to 600 A, the button was totally melted, allowing liquid specimen to pour into the mold cavity. The cast rods, 1.3 cm in diameter by 7.5 cm long, showed some surface defects (cold-shuts and cracks), many internal cracks which formed during the cooling of these very brittle materials, and fine-scale interdendritic shrinkage porosity. However the bodies of the rods had a fine microstructure and were uniform, so that an adequate number of specimens for these studies could be sectioned from these rods.

Specimen Chemistry

Chemical analyses of the cast samples show a linear relationship between the loss of Ga during melting and composition. The Ga losses (Fig. 2) are a function of the liquidus temperatures of the individual samples. The liquidus temperature drops from 1900°C, the melting point of pure V, to approximately 1600°C for the V-33Ga specimen. Thus in V-Ga specimens the temperature needed to melt the alloy completely decreased with increasing Ga, and accordingly the loss of Ga during melting also decreased. Approximately 15% excess Ga was required at the low-Ga end of the composition range of interest, whereas only 2.5% excess Ga was needed to maintain the composition of the V-37Ga sample.

V and Ga used in the specimen preparation were 99.95% and 99.99% pure respectively. Impurities (in weight percent) in the V were 0.01 Al, 0.03 Cu, 0.001 Fe, 0.001 Mn, 0.0001

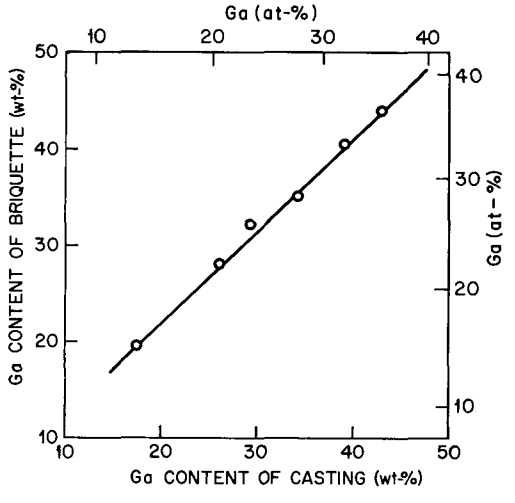

Fig. 2—The loss of Ga during arc-melting and casting of V-Ga specimens

Mg, 0.001 C, 0.001 N, and 0.011 O and in the Ga were 0.0001 Al, 0.001 Cu, 0.001 Hg, 0.00001 Mg, and 0.0001 Pb. Cu was analyzed by atomic absorption; C, N, and O in V were analyzed by vacuum fusion; and rest of the elements were analyzed by spectrochemical means.

Data from the chemical analyses of both cast and heat-treated specimens are shown in Table 2. More detailed analytical data were collected for specimens near the stoichiometric composition (V-23.3Ga, V-25.6Ga, and V-27.5Ga). The Cu contents, determined by atomic absorption, were increased above that of the pure V stock in only two specimens: V-17.9Ga and V-28.2Ga. The Cu contamination in these two specimens was introduced during arc melting. The increase in Si in the heat-treated specimens is probably a result of SiC contamination from the cutoff wheels used in sectioning the rods prior to the heat treatment. The other impurities remained at acceptably low levels. However these are spectrochemical determinations which are at best semiquantitative, since no suitable standard materials were available for direct comparisons. A Nb container was used in the high-temperature heat treatment, and accordingly the specimens were checked by spectrochemical analysis for Nb contamination. Nb impurity levels were below the detection limit of the analytical method in all specimens.

Heat Treatment

To remove the chemical gradients associated with the dendritic solidification structure of the cast specimens, it is necessary to homogenize these materials at high temperatures in the α phase field. The V-Ga materials are reactive and thus cannot be homogenized in evacuated silica capsules at the required temperatures without extensive contamination. The loss of Ga by volatilization prevents the use of a vacuum furnace for these high-temperature heat treatments. A workable procedure was devised by packing the specimens in a bed of particles of the same composition in a closed refractory metal container and conducting the high-temperature homogenization heat treatment in an argon atmosphere.

This induction heat-treating system is shown in the schematic diagram of Fig. 3. The system essentially consists of a Nb susceptor supported by a Nb stand and enclosed by a water-cooled silica tube. The silica tube is closed by a brass header provided with a windlass for lowering and raising the sample container, a thermocouple for temperature control and measurement, and a vacuum port for purging the system. The Nb specimen container is hung from a Nb rod connected to the windlass by a thin wire. By this mechanism the Nb specimen container can be positioned inside the Nb susceptor (2.5-cm diameter, 12.5-cm length, and 0.2-cm wall thickness) for heating, and the container can be removed from the hot zone for rapid cooling. In this Nb container the specimens were packed in a bed of particles of the same alloy composition for heat treatment. The specimen container was heated in high-purity argon by radiation from the Nb susceptor, which was heated inductively by a 20-kW 10-kHz motor-generator unit. With proper coil inductance the 1400°C temperature was attained using only 3 to 4 kW. The susceptor was in a chamber formed by two vertical cylindrical layers of Nb foil and a layer of fibrous zirconia near the wall of the water-cooled silica tube and by alternate layers of Nb and layers of fibrous zirconia below the stand. This cylindrical chamber was open at the top, but three Nb radiation disks were attached to the Nb rod in such a way as to close the chamber when the specimen container was in place. By this arrangement the

Table 2
Chemical Analyses of Samples

Material Designation (at-% Ga) and Heat Treatment	Major Constituents (wt-%)		Impurity Elements (wt-%)						
	V*	Ga	Al†	Cu‡	Cu†	Fe†	Mn†	Pb†	Si†
V-13.3Ga; cast	82.6	17.4	—	0.032	—	—	—	—	—
V-17.9Ga; cast	77.0	23.0	—	0.069	—	—	—	—	—
V-20.5Ga; cast	73.9	26.1	—	0.029	—	—	—	—	—
V-21.9Ga; cast	72.3	27.7	—	0.031	—	—	—	—	—
V-23.3Ga; cast	70.6	29.4	0.05	0.024	0.3	0.05	0.001	0.001	0.001
V-23.3Ga; homogenized at 1400°C for 4 hr and annealed at 1150°C for 7 hr.	—	—	0.05	—	0.01	0.05	0.001	0.01	0.3
V-25.6Ga; cast	68.0	32.0	0.05	0.036	0.3	0.05	0.001	0.001	0.001
V-25.6Ga; homogenized at 1400°C for 4 hr and annealed at 1150°C for 7 hr.	—	—	0.05	—	0.01	0.05	0.001	0.0001	0.3
V-27.5Ga; cast	65.8	34.2	0.05	0.03	0.3	0.05	0.001	Undetected	0.001
V-27.5Ga; homogenized at 1400°C for 4 hr and annealed at 1150°C for 7 hr.	—	—	0.05	—	0.05	0.05	0.001	0.0001	0.01
V-28.2Ga; cast	65.1	34.9	—	0.35	—	—	—	—	—
V-31.8Ga; cast	61.0	39.0	—	0.044	—	—	—	—	—
V-35.6Ga; cast	56.9	43.1	—	0.02	—	—	—	—	—
V-37.1Ga; cast	55.3	44.7	—	0.02	—	—	—	—	—

*Wet chemical method.
†Spectrochemical method.
‡Atomic absorption.
—Not analyzed.

temperature was made uniform within the susceptor chamber. The furnace temperature was controlled and read by a Pt/Pt-13%Rh thermocouple attached to the side of the specimen container.

Because of the decrease of solidus temperature with increasing Ga content, the homogenizing heat treatments were selected as 4 hours at 1400°C for specimens containing 13 through 29 at-% Ga, 5 hours at 1275°C for specimens containing 31.8 at-% Ga, and 6 hours at 1200°C for specimens containing 35.6 and 37.1 at-% Ga. At the end of the homogenization heat treatments the specimens were rapidly cooled by removing the container from the induction zone. The temperature dropped from 1200-1400°C to 500-700°C in about 1 minute, generating a fine β structure by the solid-state α-to-β transformation, thus yielding transformed specimens.

The transformed specimens were cut into two parts; one part was retained for microstructural studies and superconductivity measurements, and the other part was subjected to additional annealing in the β field to eliminate fine-scale transformation segregation arising from the α-to-β transformation. For the latter purpose the annealing

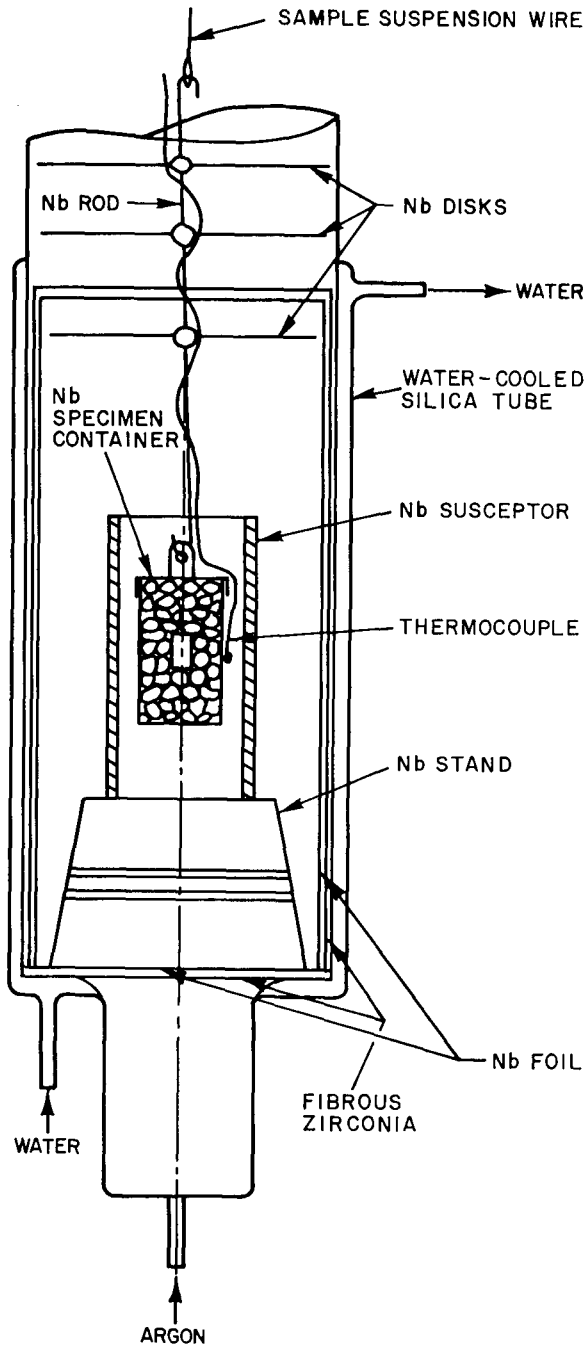

Fig. 3—Induction annealing furnace for the high-temperature homogenization and annealing

conditions were chosen as 7 hours at 1150°C for specimens containing 13 through 29 at-% Ga, and 7 hours at 990°C for specimens containing 30 through 37 at-% Ga. These annealed specimens were used for microstructural studies and for microhardness, lattice-parameter, and superconductivity measurements.

Selected specimens were subjected to long-term anneals in evacuated silica capsules for a redetermination of the composition limits of the β phase and for long-range-order studies. Si contamination from the silica capsules was negligible during the relatively low temperature (700 to 800°C) long-term anneals required for these studies.

Microstructure and Microhardness

Microstructure was studied by standard metallographic techniques. These studies were augmented by microhardness measurements, electron microprobe analyses, and spectrochemical analyses. Whenever possible, microhardness measurements were used to identify the α and β phases.

Excessive crack formation was observed in metallographic specimens mounted under pressure in a thermal-setting plastic. This problem was minimized by mounting the specimens in an epoxy resin. Standard grinding and polishing techniques were used for preparing the metallographic specimens, but the coarsest SiC paper used for grinding the mounted specimens was 320 grit size, because any coarser grit size produced excessive cracking and chipping of these brittle specimens. The specimens were polished with α and γ alumina on suitable cloth-covered wheels.

A variety of metallographic etchants proposed by other investigators were evaluated. None was completely satisfactory, but the modified solutions that we found most useful are listed in Table 3 with a brief notation of their characteristics. These characteristics are illustrated by the photomicrographs of Fig. 4, as well as by those in other sections of this report. The hydroxide-peroxide etchant delineates boundaries between phases (α, β, γ, and the impurity phase) but not the grain boundaries within the β phase. The structure of a not fully equilibrated V-13.3Ga specimen (Fig. 4a) illustrates this. The β phase, which forms a continuous network along the α grain boundaries and also forms individual platelets within the α grains, is clearly delineated in the α matrix. The mixtures of nitric acid, hydrofluoric acid, and water are more successful in revealing the structure of the β phase. Figures 4b and 4c show the same area of a transformed V-28.2Ga specimen etched with two mixtures of these acids. The $1HNO_3$:10HF:$30H_2O$ mixture reveals many of the β-phase grain boundaries, a few subboundaries, and a linear veining pattern ascribed to variations in the Ga content of the β phase arising from the α-to-β transformation; this etchant accentuates the particle population of the impurity phase. Figure 4c shows the effect of this mixed-acid etch, now in the proportion $5HNO_3$, 2HF, and $30H_2O$, on the same structure. The β grain boundaries and subboundaries are more distinct and the veining is revealed but the population of impurity-phase particles seems low. Examination of this etched structure at high magnifications revealed two populations of impurity particles, the first strongly attacked (darkly colored) and the others lightly attacked. Thus the impurities may generate particles of two phases or of one phase with variable composition.

Table 3
Metallographic Etching Solutions

Compositions* (parts by volume)	Etching Time (min)	Characteristics
$4NH_4OH$, $1H_2O_2$	2-4	Delineates phase boundaries, particularly α/β boundaries.
$1HNO_3$, 10HF, $30H_2O$†	2-4	Reveals β grain boundaries.†
$5HNO_3$, 2HF, $30H_2O$†	3-10	Reveals microstructural details, such as subboundaries and dislocations. This etch is sensitive to crystallographic orientation of the grains.†

*The concentrations of each of the chemical reagents used in composing the etching solutions were 28 to 30% NH_3, 70 to 71% HNO_3, 48% HF, and 3% H_2O_2.
†Surface stains form rather rapidly on the etched specimen. This staining can be prevented by dipping the etched specimens in a $1NH_4OH:10H_2O$ solution for 30 seconds.

The etching characteristics of the β grains in the mixed-acid solutions show an orientation dependence. For some orientations this type of etchant reveals fine-scale structural elements. The annealed specimen of V-25.6Ga shown in Fig. 5 was etched in the $5HNO_3:2HF:30H_2O$ solution. Subboundaries and dislocation pits are evident in one β grain but remain completely undelineated in the others.

Distinguishing the α, β, and γ phases in metallographic sections was not always easy. When the specimens contained a substantial amount of a second phase, it was identified by x-ray diffraction. Similarly, when the α and β phases occurred in coarse structures, microhardness measurements were used to distinguish these two phases. For a 100-g indentation load, the hardness of the α phase ranged from 350 to 570 kg/mm^2 as the gallium content of the sample increased from 17.9 to 35.6 at-%. The hardness of the β phase was significantly higher: 990 to 1090 kg/mm^2. But for most specimens of interest in these studies, the second phase in the β matrix was a minor constituent, and metallographic identification was required. The γ phase, being hexagonal, was detected in unetched specimens by its optical activity in polarized light. The impurity phase was inactive, as were the cubic α and β phases. None of the etchants used produced distinctive colorations of the phases. Instead there were only slight differences in the etching characteristics and reflectivity of the phases to be used for identification. At high optical magnifications the α phase appeared more heavily attacked than the β phase, and the impurity phase showed a faint pink color.

X-ray Diffraction Determinations of the Lattice Parameter and Long-Range Order

For all diffraction measurements the specimens were powdered to pass through a 325-mesh (44-μm) sieve. In our experiments sharp x-ray-diffraction lines were observed in Debye-Scherrer powder patterns of the brittle A15 phase samples. The sharp diffraction profile made it possible to determine the lattice parameter of these samples with an accuracy of ±0.0005 Å.

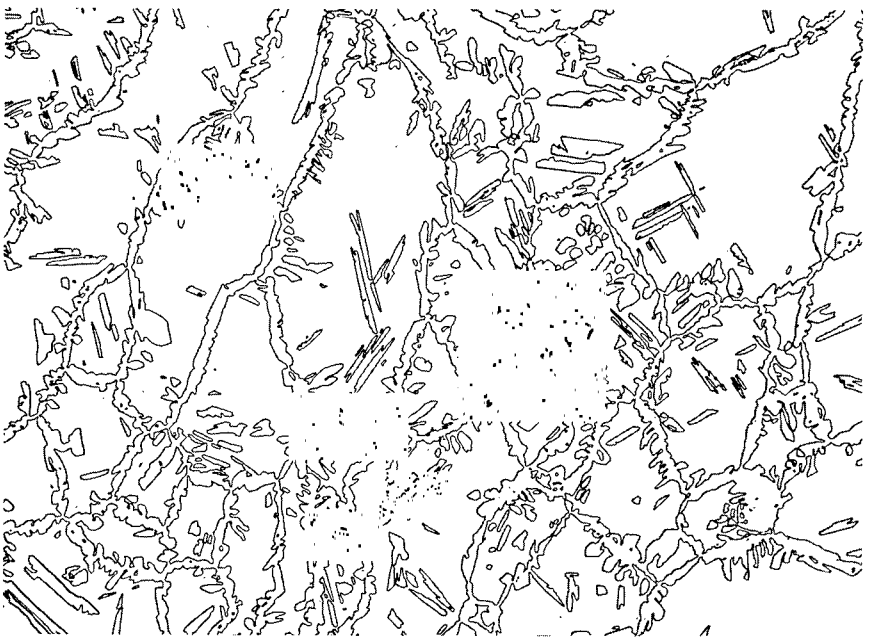

(a) V-13.3Ga etched with $4NH_4OH:1H_2O_2$ for 3 minutes. The β phase is a continuous network at α-grain boundaries and is also platelets within the grains. Magnification 150X.

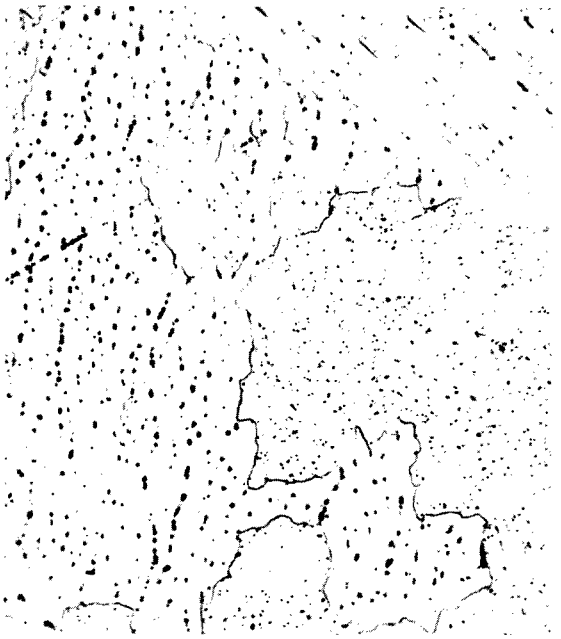

(b) V-28.2Ga etched with $1HNO_3:10HF:30H_2O$ for 3 minutes. The transformed β-phase grains contain impurity-phase particles and a network of weakly delineated subboundaries. Magnification 500X.

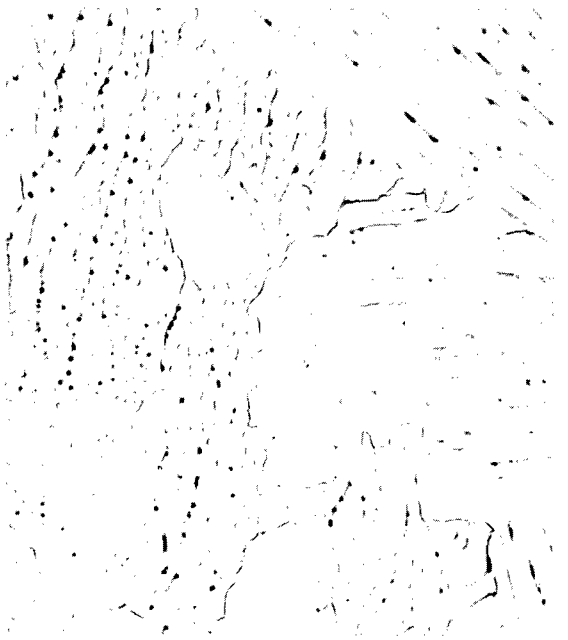

(c) Same area of the V-28.2Ga specimen shown in Fig. 4b but etched with $5HNO_3:2HF:30H_2O$ for 7 minutes. Magnification 500X.

Fig. 4—Microstructures illustrating the characteristics of the etching solutions of Table 3

Fig. 5—Subboundaries and dislocation etch pits in an annealed V-25.6Ga specimen etched with $5HNO_3$:2HF:$30H_2O$ for 7 minutes. Magnification 1000X.

Three samples (V-23.3Ga, V-25.6Ga, and V-27.5Ga), with high transition temperatures were selected for long-range-order studies. X-ray measurements of long-range order were made on these three compositions in each of the three conditions: cast, transformed, and annealed. X-ray integrated line intensities from the 110, 200, 210, and 211 reflections were measured with a diffractometer equipped with a crystal monochromator. Each peak was scanned for an angular distance of 3 degrees (in 2θ) at a scanning speed of 1/8 degree per minute. All intensities were measured with a xenon proportional counter operated with pulse-height analysis, and the accumulated counts were recorded in digital form. Background x-ray intensities were measured within 2% probable error at the beginning and end of each scan. Anomalous-dispersion corrections [3] and temperature corrections were applied for V and Ga. The Lorentz polarization and multiplicity factors were incorporated in the intensity calculations.

Superconductivity Measurements

Normal-to-superconducting-state transitions were determined by observing the temperature dependence of the relative magnetic susceptibility of the samples using a Hartshorn-type ac mutual inductance bridge [4]. The temperature at the susceptibility point midway between the susceptibility values of the fully superconducting state and the normal state defines the superconducting transition temperature T_0. Temperatures were determined with a germanium resistance thermometer. The cryostat used in the measurements of the superconducting properties of these alloys is shown schematically in Fig. 6. The cryostat permits reloading of samples while leaving the measuring coil in situ.

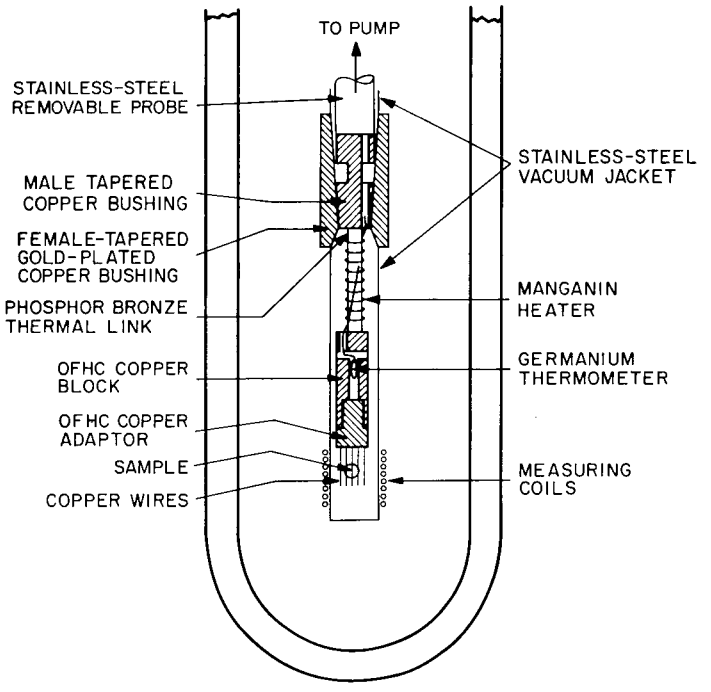

Fig. 6—Low-temperature cryostat used in measuring the superconducting transition temperature

A female-tapered gold-plated copper bushing joins the two segments of a thin-walled stainless-steel vacuum jacket. The corresponding male taper, again made of copper to assure good thermal contact, joins the removable stainless-steel probe to the rest of the sample-holding apparatus. Hard-soldered to the male taper is a phosphor bronze thermal link, around which a Manganin heater is wrapped over the leads to the germanium thermometer, which in turn is imbedded inside an OFHC (oxygen-free high-conductivity) copper block. An OFHC copper adaptor is threaded into the block using a zinc oxide paste to provide good thermal contact. Welded to the adaptor are several hundred 0.005-inch-diameter copper wires, and the sample is emeshed inside these with more zinc oxide paste and bundled with cotton thread. The measuring coils are wound directly on the stainless-steel jacket, and the entire assembly is loaded into the dewar system. The leads to the heater and the thermometer are brought up through the probe to room-temperature connectors after passing through several wads of copper wool which act as radiation baffles. A pumping port is affixed to the wall of the stainless-steel jacket outside the dewar.

RESULTS AND DISCUSSIONS

Cast Microstructures

The cast 1.3-cm-diameter rods all had uniform and fine microstructures. However these microstructures displayed evidence of chemical segregation. This segregation arose during solidification and is of two types: fine-scale dendritic patterns and a more diffuse long-range radial gradient. Solidification, as indicated by the phase equilibria of Fig. 1, proceeds by the formation of dendrites of the α phase, which are of lower Ga content

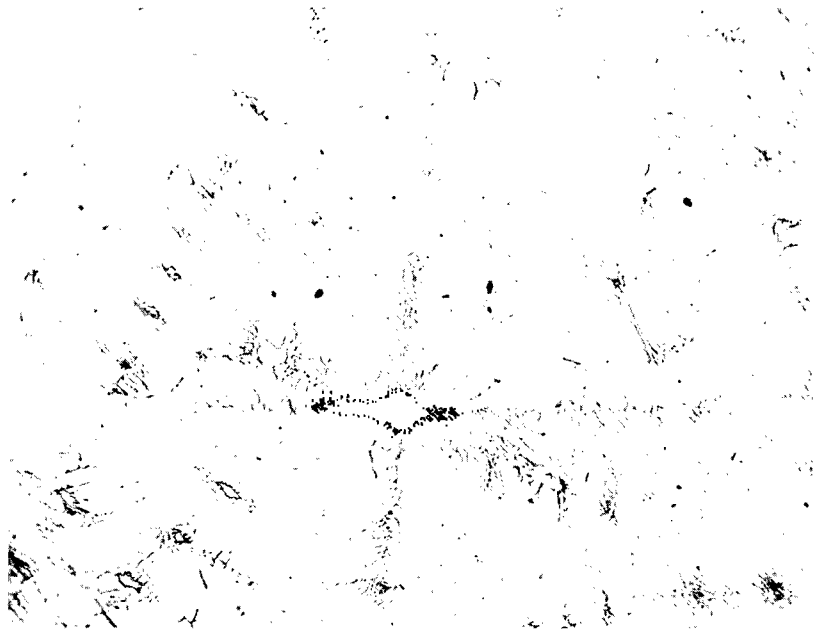

Fig. 7—Microstructure of a cast V-21.9Ga specimen etched with NH_4OH:1H_2O_2 for 3 minutes. Dendritic segregation of Ga and the α-phase dendrite cores in the β-phase matrix are revealed by the etchant. Magnification 250X.

than the liquid. As the temperature falls, these dendrites grow inward toward the centerline of the rod by accreting more solid of increasing Ga content from a liquid that is also increasing in Ga content. Thus the solidification produces a single-phase α material containing fine dendritic cores of low Ga content and a gradient of increasing Ga content from the rod surface to the rod center.

The α phase remains stable to room temperature, transforms to the β phase, or is retained as a metastable phase depending on the Ga content of the α phase and the cooling rate. Thus the lower Ga specimens (V-13.3Ga, and V-17.9Ga) contained stable α-phase dendrite cores. Specimens of higher Ga content (V-21.9Ga and V-23.3Ga) retain some α phase in the dendrite cores, but most of the structure transforms to the β phase on cooling. An example of the cast structure of the V-21.9Ga material is shown in Fig. 7. Here the matrix has transformed to the β phase on cooling, but the Ga-lean dendrite cores have remained in the α phase. The patterns of fine lines which make the extended dendritic pattern visible are a consequence of the α-to-β transformation and reveal the microsegregation of Ga generated in this process. At higher Ga contents (V-25.6Ga and V-27.5Ga) no α phase is retained in the dendritic cores of the cast structure. However, when etched properly, the dendritic pattern of the Ga segregation becomes evident. This pattern is illustrated by the photomicrograph of the cast V-25.6Ga specimen in Fig. 8. When the Ga content is increased further, the radial composition gradient becomes evident, because the core of the rod remains with α phase and only a thin surface layer transforms to the β phase on cooling. This structure of a high-gallium alloy (V-31.8Ga) is shown in Fig. 9. In this micrograph the retained α phase is the darker phase. The peroxide-hydroxide etch reveals the grain boundaries within this phase, and some evidence of the solidification segregation is revealed by the stain pattern. The structure within the transformed β-phase surface layer is completely undifferentiated by the etch, but the

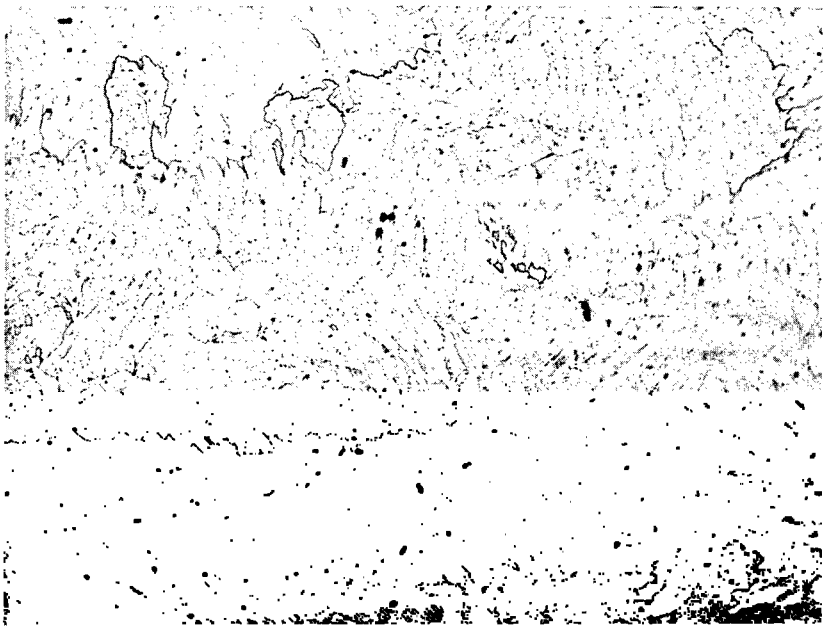

Fig. 8—Microstructure of a cast V-25.6Ga specimen etched with $5HNO_3$:2HF:$30H_2O$ for 6 minutes. The etch delineates the boundaries between β-phase grains and the dendritic segregation patterns within these grains. Magnification 150X.

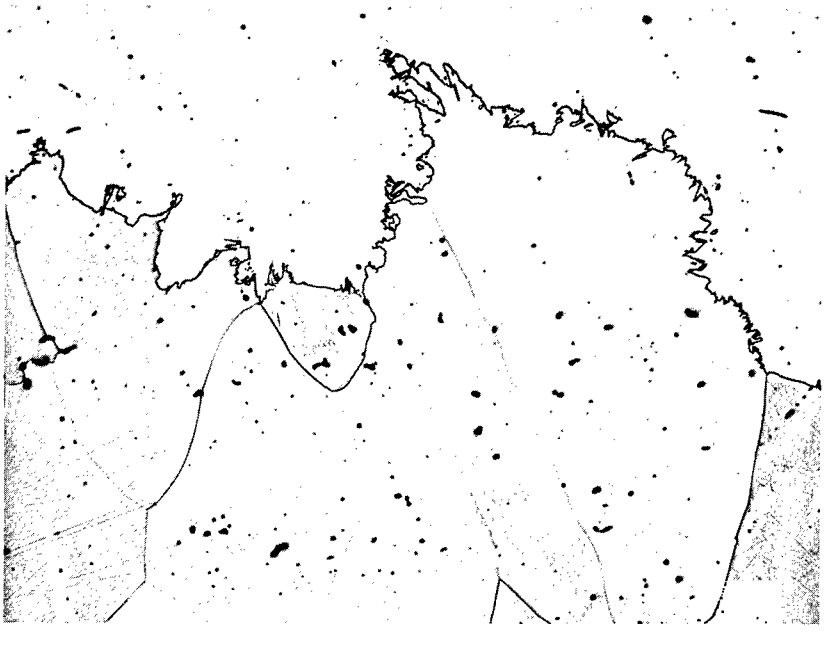

Fig. 9—Microstructure at the interface between the α-phase core (dark) and the β-phase rim (light) of a cast V-31.8Ga specimen etched with $4NH_4OH$:$1H_2O_2$ for 3 minutes. This restricted α-to-β transformation is evidence of the radial segregation of Ga: low in the peripheral region (β phase) and high in the core (α phase). Magnification 150X.

jagged α-to-β transformation interface is clearly delineated. The Ga-lean α phase formed at the surface transforms to the β phase, whereas the Ga-rich α phase in the body of the rod is retained as a metastable α phase. The marked decrease in the kinetics of the α-to-β transformation with increasing Ga content of the α phase produces this structure and makes evident the radial inhomogeneity in the Ga distribution.

Although the radial segregation is clearly discerned in the microstructure of the high-Ga specimens, where the width of the liquid-plus-α-phase field is broadest, enhancing this segregation, we must also assume that similar, but smaller, gradients exist in the other specimens of lower Ga content. Since this segregation extends over distances comparable to the radius of the rod, it cannot be eliminated completely by homogenization heat treatments of reasonable duration. The dendritic segregation, on the other hand, is on a much finer scale and can be eradicated by a high-temperature homogenization heat treatment.

Homogenization

Although several previous studies [5-7] of V_3Ga used heat treatments to homogenize the cast specimens at temperatures within the β-phase range (650 to 1150°C), we have found these treatments inadequate. Figure 10 is a photomicrograph of the microstructure of a V-25.6Ga specimen that was annealed for 3 weeks at 650°C. The dendritic segregation pattern is quite prominent and not significantly different from that observed in the as-cast specimen in Fig. 8. Similarly a specimen of V-21.9Ga annealed for 100 hours at 1000°C shows the distinct dendritic pattern of the cast structure (Fig. 11). The α-phase dendrite cores have been transformed to the β phase, but the Ga segregation from the solidification process has not been eliminated.

Each of these specimens was sealed in evacuated silica capsules for these prolonged heat treatments. Not unexpectedly the V-21.9Ga specimen annealed at 1000°C showed evidence of reaction with the silica capsule, and extensive contamination resulted. The consequences of this contamination were formation of a surface layer of a new phase containing Si (verified by spectrochemical analysis), retention of the general nature of the α phase, and a change in the response of this phase to the etch. No such contamination was evident in the microstructure of the V-25.6Ga specimen annealed for 3 weeks at 650°C. Thus for prolonged anneals at 800°C or lower we have used the convenience of the silica capsule. For all higher temperature heat treatments we have used pack annealing in the induction furnace.

The effectiveness of our heat-treating procedure can be seen by comparison of photomicrographs. The cast materials showed dendritic segregation which was effectively revealed by the mixed-acid etchant; Figs. 7, 8, 10, and 11 are examples of this microstructure. The high-temperature homogenization in the α-phase field eliminates the dendritic segregation, but cooling through the α-to-β transformation generates a fine-scale segregation pattern. This structure, characteristic of all of the transformed specimens, is illustrated in Figs. 4b and 4c. Annealing at high temperature within the β-phase field rapidly removes this last form of segregation. The photomicrograph of Fig. 12 shows the annealed structure. This is the same V-28.2Ga alloy shown in Fig. 4c after annealing at 1150°C for 5 hours. The specimen was etched with the same mixed-acid solution. All vestiges of the transformation structure have been eliminated, and only the spheroidized impurity-phase particles are seen in the large-grained homogeneous β matrix. All annealed specimens showed this type of microstructure.

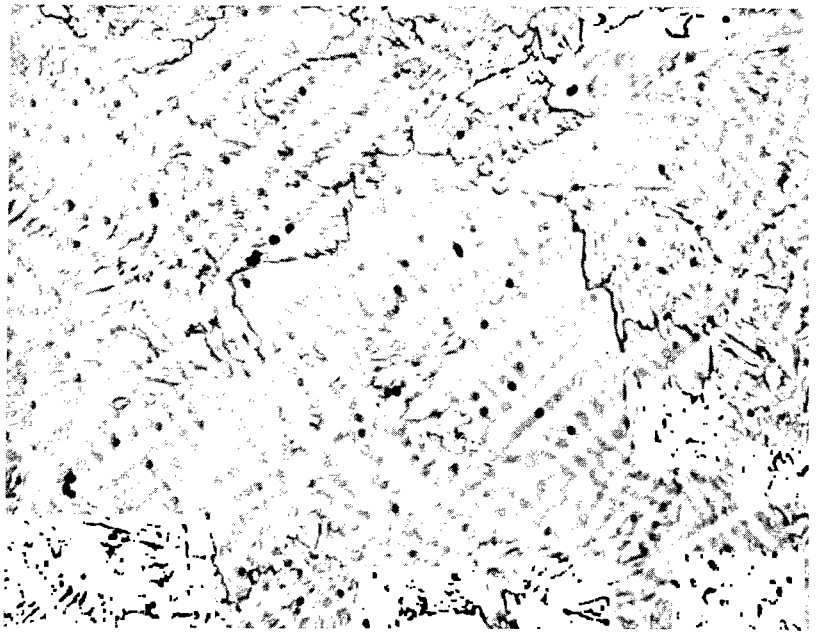

Fig. 10—Dendritic segregation in the microstructure of a V-25.6Ga specimen etched with $5HNO_3$:2HF:$30H_2O$ for 6 minutes after annealing at 650°C for 3 weeks. Magnification 100X.

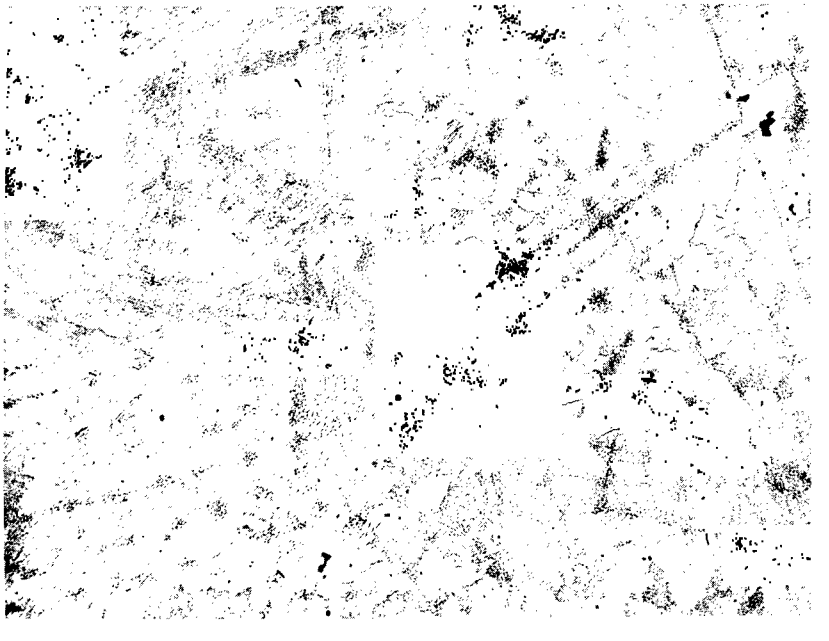

Fig. 11—Dendritic segregation in the microstructure of a V-21.9Ga specimen etched with $5HNO_3$:2HF:$30H_2O$ for 6 minutes after annealing at 1000°C for 100 hours. Magnification 100X.

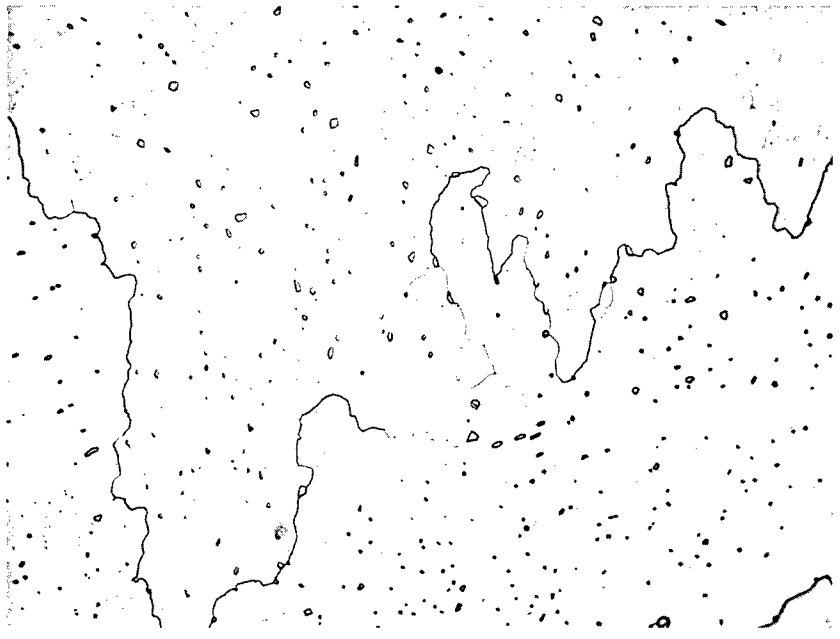

Fig. 12—The β-phase microstructure of a V-28.2Ga specimen etched with $5HNO_3$:2HF:$30H_2O$ for 6 minutes after homogenizing at 1400°C for 6 hours and annealing at 1150°C for 5 hours. The large grains, containing spherodized impurity particles, show no evidence of segregation. Magnification 250X.

The impurity phase was present in all specimens. In the cast materials it appeared in the microstructures as filaments or films at β-grain boundaries. In the high-Ga alloys, where the α phase was retained in parts of the casting, the impurity phase was not evident in the α-phase matrix, but it was present in the portions that had transformed. This suggests a solubility in the α phase of the impurities responsible for the formation of this phase. In all of the transformed specimens the distribution of the impurity-phase particles and the veining conform to the same pattern (Figs. 4b and 4c), again suggesting a rejection of the impurity phase during the transformation. On annealing, the impurity particles spheroidize (Fig. 12) and remain on grain boundaries or on subboundaries (Fig. 5).

Several attempts were made to identify the impurity phase—its origin, composition, and crystal structure. No correlation was found between the impurity-phase population and spectrochemical indications of high Cu and Si concentrations. Electron-probe microanalyses supported this, for no concentration of Cu or Si or of W or Fe was detected in the particles. These analyses did show a lower Ga content in the particles than in the matrix, a typical example being 15 to 17 at-% Ga in the particles and 22 at-% Ga in the matrix.

The concentration of the impurity phase was too small to yield discernible lines in the x-ray powder patterns, and attempts to extract and concentrate the phase by chemical and mechanical means were unsuccessful. The impurity phase is hard and brittle, though less brittle than the β phase, and shows no activity under polarized light.

Philipsborn and Laves [8] observed that when the A15 phases Ti_3Au, V_3Pt, and V_3Au were remelted in an arc furnace in argon containing small amounts of oxygen, nitrogen, or carbon, a Cu_3Au-type phase occurred along with the A15 phase. The impurity phase in our V-Ga samples is most probably a cubic Cu_3Au-type phase stabilized by small amounts of oxygen, nitrogen, or carbon.

Microhardness

According to Junod et al. [6] the microhardness of the β phase is minimum at the stoichiometric composition and reaches high values near the composition limits of β phase field. The reported microhardness decreases from 1630 ± 40 kg/mm^2 for 20 at-% Ga to 1000 ± 20 kg/mm^2 for stoichiometric composition and then increases again to 1500 ± 50 kg/mm^2 for 30 at-% Ga. However our measurements of annealed specimens show the microhardness of the β phase across the A15 phase field remaining essentially constant at about 900 kg/mm^2 for a 300-g load and about 1000 kg/mm^2 for a 100-g load (Table 4). The formation of microcracks, particularly at the 300-g load, may be responsible for slightly lower values measured at this higher indenter loading. This uniformity in hardness is contrary to the suggestion of Matthias [9] and the results reported by Junod et al. [6].

Lattice Parameters

Changes in the lattice parameter a_0 of a material give a measure of modifications in the atomic interaction parameters and bond lengths, which parameters and lengths influence electron-phonon interactions and superconducting properties. Moreover deviations from linear relationships in the lattice parameter as a function of composition may indicate a change in the defect state of the material. For the V-Ga system the lattice parameter of the β phase shows a large change with composition. Thus a well-defined lattice-parameter curve based on chemically analyzed specimens permits the establishment of the Ga content for specimens of intermediate compositions. The Ga content is

Table 4
Microhardness of V_3Ga (A15) Annealed Specimens

Specimen Designation	Indentation Load (g)	Microhardness (kg/mm^2)
V-21.9Ga	100	1003-1004
	300	887- 908
V-23.3Ga	100	1033-1056
	300	890- 970
V-25.6Ga	100	988-1094
	300	898- 916
V-27.5Ga	100	989-1026
	300	894- 901
V-28.2Ga	100	989-1056
	300	869- 890

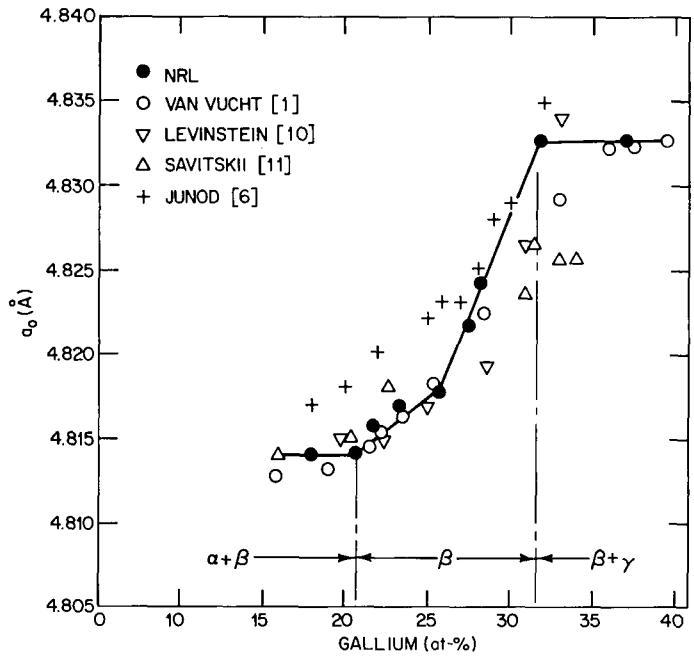

Fig. 13—The lattice parameter, a_0 of the β phase of the V-Ga system as a function of composition

determined to within ±0.25 at-% on the Ga-rich side and to within ±0.5 at-% on the V-rich side.

Although a number of investigators reported the lattice parameter of the β phase as a function of composition, agreement among these sets of data is lacking. Therefore in the present investigation the lattice parameter of the β phase across its composition range was measured carefully using the well-annealed specimens. The measured lattice parameters are compared in Fig. 13 with four similar sets of data selected from the literature [1,6,10,11]. It is evident that our a_0 values are in closest agreement with those of van Vucht et al. [1]. Our data indicate two line segments of different slopes intersecting near the stoichiometric V_3Ga composition. Among the other results given for this system, only the data of Levinstein et al. [10] show a sharp break in the variation of lattice parameter as a function of composition. According to their results this change of slope occurs near 28 at-% Ga. The fact that their data show a change in slope away from the stoichiometric composition may be related to the uncertainties in the chemical composition of their alloys, since these compositions were based on the masses of V and Ga reacted rather than on the chemical analysis of the final alloys. The data of van Vucht et al. [1] show a distinct change in slope near the stoichiometric V_3Ga composition—even though these authors drew a smooth S-shaped curve through their data. Kuznetsova and Zhdanov [12] have confirmed from their density measurements and existing lattice-parameter data that these two different slopes in V-rich and Ga-rich alloys correspond to the substitution of excess V in Ga lattice positions (at cube corners and at the center of the cube) and to substitution of excess Ga in V chains, respectively. Our lattice-parameter data support this observation.

The recent density measurements of the β phase by Junod et al. [6] further support the substitution mechanisms of excess Ga in V sites and excess V in Ga sites respectively. Junod et al. mentioned in their paper that their lattice-parameter measurements were in close agreement with the results of Savitskii et al. [11]. However, when the results of Junod and Savitskii are compared on the enlarged ordinate scale of Fig. 13, the disparity in these two sets of data becomes evident. Savitskii's results show a linear relationship across the entire composition range, but his data from high Ga specimens are significantly lower than those of Junod or ours. On the other hand, Junod's results suggest a break around 27 at-% Ga, but at lower Ga contents his data are significantly higher than ours.

Composition Limits of the β Phase

Based on lattice parameters and metallographic observations, a modification of the composition limits of the β phase as defined by van Vucht [1] is presented here. Three specimens, V-13.3Ga, V-17.9Ga, and V-20.5Ga, in the vanadium-rich end of the β-phase field (Fig. 14) were annealed at 1000, 1150, 1200, and 1225°C, after high temperature homogenization at 1400°C. The metallographic examinations of V-13.3Ga and V-17.9Ga, annealed at 1150 and 1200°C respectively and then cooled rapidly, showed only the α phase. Metallographic determinations of the relative amounts of the α and β phases in V-13.3Ga, V-17.9Ga and V-20.5Ga annealed at 1000, 1150, and 1225°C along with lattice-parameter measurements provided the means to establish the modified α-phase and β-phase boundaries. At 1000°C the α-phase field terminates around 11 at-% Ga and the β-phase field starts at 21 at-% Ga. The α-phase and β-phase boundaries as reported by van Vucht [1] (Fig. 1) are shown by dashed lines in Fig. 14. The range of occurrence

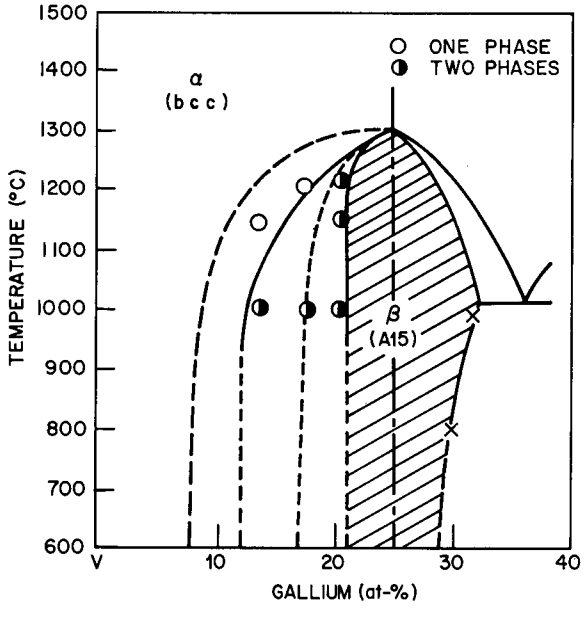

Fig. 14—Modified composition limits of the β phase of the V-Ga system. The β-phase boundaries reported by van Vucht et al. [1] are shown as dashed lines.

of the β phase at 1000°C is from 21.0 to 31.5 at-% Ga, and this range is narrower than that reported by van Vucht [1].

Our determination of the Ga-rich boundary of the β phase field agrees well with that of van Vucht. From lattice-parameter measurements we established that the β-phase boundary moves toward lower Ga content as the temperature decreases from 990 to 800°C. Transformed specimens of V-31.8Ga and V-37.1Ga were annealed for 7 hours at 990°C and 672 hours at 800°C respectively. Measurements of the lattice parameters of the β phase in these β-plus-γ specimens gave 4.8325 Å for the specimen equilibrated at 990°C and 4.8275 Å for the specimen equilibrated at 800°C. Using the data of Fig. 13, we find these lattice parameters indicate Ga contents of 31.5 at-% at 990°C and 29.5 at-% at 800°C. These values, indicated by crosses in Fig. 14, are in complete agreement with the earlier results of van Vucht.

Long-Range-Order Study

In a number of A_3B compounds with A15 structures the highest superconducting transition temperatures are attained when the compounds are stoichiometric and completely ordered [13,14]. Therefore a processing method which produces a perfectly ordered material is desired to achieve optimum superconducting properties. In the perfectly ordered A15 structure the A atoms, transition-metal atoms, occupy pairs of "A sites" on the cube faces, and the B atoms occupy "B sites" at the cube corners and the body-centered position. When every A and B site is occupied by the proper atom, the material is in the perfectly ordered condition. It has been suggested in the literature that there is an optimum annealing temperature at which nearly perfect order can be attained in a relatively short period of time. The lack of definition of this optimum temperature however has led many investigators to perform the ordering anneal at low temperatures—a process requiring an inordinately long time. For example, heat treatments for ordering V_3Ga that have been reported in the literature range from 600 to 900°C for periods of 1 to 3 weeks.

Because of the appreciable differences in atomic-scattering factors of V and Ga, the degree of order in V_3Ga phase can be studied conveniently by X-ray-diffraction methods. For these studies three compositions, V-23.3Ga, V-25.6Ga, and V-27.5Ga, were selected. Samples of each of the compositions in the cast, transformed, and annealed conditions were crushed to powder for these measurements.

In the study of long-range order the integrated intensity (I) from the powder specimens is related to the structure factor according to the relationship $I \propto m(Lp)|F|^2$, where m is the multiplicity, Lp is the Lorentz-polarization factor, and F is the structure factor. Again the structure factor F depends on the degree of order S, the atomic scattering factors f_A and f_B, and the atom fractions X_A and X_B. Thus for a specific composition the changes in degree of order S can be measured by the changes in integrated intensity. To calculate the integrated intensities for specimens of different compositions subjected to a variety of processing treatments, a knowledge of the contributions of the degree of order S and the atomic fractions X_V and X_{Ga} to the structure factor F is necessary.

The degree of order S is the usual Bragg-Williams parameter

$$S = (r_V - X_V)/(1 - Y_V) = (r_{Ga} - X_{Ga})/(1 - Y_{Ga}),$$

where r_V and r_{Ga} are the fractions of V and Ga sites occupied by the V and Ga atoms respectively, X_V and X_{Ga} are atomic fractions of V and Ga present in the sample and thus depend on the composition of the sample, and Y_V and Y_{Ga} are the fractions of V and Ga sites in the perfect V_3Ga lattice ($Y_V = 0.75$ and $Y_{Ga} = 0.25$). According to this definition the maximum degree of order S_M is, for example, 0.966 for a sample containing 72.5 at-% V and 27.5 at-% Ga. From an extension of Warren's treatment [15] of long-range order in binary compounds with A15 structure, the contributions of the degree of order and the composition to the structure factors were established. These results are presented in Table 5. For stoichiometric samples ($X_A = 0.75$ and $X_B = 0.25$) these equations reduce to the forms presented in the right-hand column, which agree with those published by van Reuth and Waterstrat [16].

The structure factor F for 110, 200, 210, and 211 reflections were calculated using the tabulated values of atomic-scattering factors [17]. Normalized calculated and measured intensities are presented in Table 6. The degree of order of the V_3Ga sample is established by comparing the measured intensities with the intensities calculated for specific values of S. Here S_m, shown in the second column, corresponds to the maximum degree of long-range order that each of the three compositions can attain, and S_p and S_d correspond respectively to partial long-range order and disorder (no long-range order). Calculated intensity values for $S_d = 0$, $S_p = 0.9$ and S_m = value in the second column are compared with the measured values for the cast, transformed, and annealed specimens. These measured intensities indicate that the specimens show a high degree of order in all conditions.

The intensity ratios of the neighboring reflections point out the differences in the degree of order among the cast, transformed, and annealed specimens for each composition. Among the five calculated and measured relative intensity ratios presented in Table 7, the calculated (200)/(211) intensity ratios are all close to 0.48, because these two planes have identical structure factor relationships (Table 5). The 200/211 intensity ratios are slowly varying functions of composition and degree of order. Thus this ratio does not change appreciably with the changes in degree of order, and deviations from the calculated values would indicate preferred orientation in an x-ray specimen. The small scatter in the experimental 200/211 intensity ratios indicate that the powder samples show some evidence of preferred orientations.

The calculated 110/200 and 110/210 intensity ratios show an increase from disorder through maximum ordered conditions, whereas the 210/211 intensity ratios decrease. Similar trends are seen in the experimental intensity ratios of cast through annealed specimens, and within the 0.9 to 1 S-value range the changes in experimental intensity ratios are small. Here deviations from the general trends may be related to the small amount of preferred orientation present in the x-ray specimens. These ratios show that the degree of order is high in the cast specimens (S about 0.9), and this degree of order improves slightly in the transformed and the annealed specimens.

The increase in the degree of order S in the annealed specimens becomes clearer when one examines a plot of these intensity ratios against composition. In Fig. 15 both the calculated and the experimental intensity ratios of 110/200 planes show similar

Table 5
A15 Structure Factors F

Reflections	Structure Factors F	
	Nonstoichiometric Composition	Stoichiometric Composition
110	$2S(f_B - f_A)$	$2S(f_B - f_A)$
200	$S(f_B - f_A) + 4(f_A X_A + f_B X_B)$	$S(f_B - f_A) + (3f_A + f_B)$
210	$S(f_B - f_A) - 4(f_A X_A + f_B X_B)$	$S(f_B - f_A) - (3f_A + f_B)$
211	$S(f_B - f_A) + 4(f_A X_A + f_B X_B)$	$S(f_B - f_A) + (3f_A + f_B)$
220	$2S(f_B - f_A)$	$2S(f_B - f_A)$
310	$2S(f_B - f_A)$	$2S(f_B - f_A)$
222	$3S(f_B - f_A) - 4(f_A X_A + f_B X_B)$	$3S(f_B - f_A) - (3f_A + f_B)$
320	$S(f_A - f_B) + 4(f_A X_A + f_B X_B)$	$S(f_A - f_B) + (3f_A + f_B)$
321	$S(f_B - f_A) + 4(f_A X_A + f_B X_B)$	$S(f_B - f_A) + (3f_A + f_B)$
400	$2(4(f_A X_A + f_B X_B))$	$2(3f_A + f_B)$

(f_A and f_B are the atomic scattering factors of A and B atoms respectively for the corresponding $(\sin\theta)/\lambda$ values, X_A and X_B are respectively the atom fractions of A and B atoms, and S is the degree of order)

Table 6
Calculated and Measured Normalized Integrated Intensities for A15 V-Ga Specimens

Specimen Composition (at-%)	Maximum Order S_m	X-Ray Line	Calculated Intensity			Measured Intensity		
			Disorder $S_d = 0$	Partial Order $S_p = 0.9$	Maximum Order S_m	As Cast	Trans-formed	Annealed
V-23.3Ga	0.933	110	0	3.76	4.06	4.95	4.83	5.52
		200	35.17	46.41	46.89	47.60	45.13	51.26
		210	100.00	100.00	100.00	98.72	95.84	96.50
		211	72.78	97.06	98.10	100.00	100.00	100.00
V-25.6Ga	0.992	110	0	3.70	4.56	5.17	6.27	6.09
		200	35.15	46.29	47.62	49.17	50.72	47.00
		210	100.00	100.00	100.00	89.44	98.56	89.48
		211	72.81	96.91	99.79	100.00	100.00	100.00
V-27.5Ga	0.966	110	0	3.65	4.25	5.10	5.54	5.05
		200	35.13	46.19	47.13	46.07	51.09	47.65
		210	100.00	100.00	100.00	97.34	114.98	87.83
		211	72.84	96.78	98.82	100.00	100.00	100.00

Table 7
Calculated and Measured Relative Intensity Ratios for A15 V-Ga Specimens

Specimen Composition (at-%)	Maximum Order S_m	Ratio of Reflections	Calculated Ratios			Measured Ratios		
			Disorder $S_d = 0$	Partial Order $S_p = 0.9$	Maximum Order S_m	As Cast	Transformed	Annealed
V-23.3Ga	0.933	110/200	0	0.0810	0.0866	0.1040	0.1070	0.1077
		110/210	0	0.0376	0.0406	0.0501	0.0504	0.0572
		200/210	0.3517	0.4641	0.4689	0.4822	0.4709	0.5312
		200/211	0.4832	0.4782	0.4780	0.4760	0.4513	0.5126
		210/211	1.3740	1.0303	1.0194	0.9872	0.9584	0.9650
V-25.6Ga	0.992	110/200	0	0.0799	0.0958	0.1051	0.1236	0.1296
		110/210	0	0.0370	0.0456	0.0578	0.0636	0.0681
		200/210	0.3515	0.4629	0.4762	0.5498	0.5146	0.5253
		200/211	0.4828	0.4777	0.4772	0.4917	0.5072	0.4700
		210/211	1.3734	1.0319	1.0021	0.8944	0.9856	0.8948
V-27.5Ga	0.966	110/200	0	0.0790	0.0902	0.1107	0.1085	0.1060
		110/210	0	0.0365	0.0425	0.0524	0.0482	0.0575
		200/210	0.3513	0.4619	0.4713	0.4733	0.4443	0.5425
		200/211	0.4823	0.4773	0.4769	0.4607	0.5109	0.4765
		210/211	1.3729	1.0333	1.0119	0.9734	1.1498	0.8783

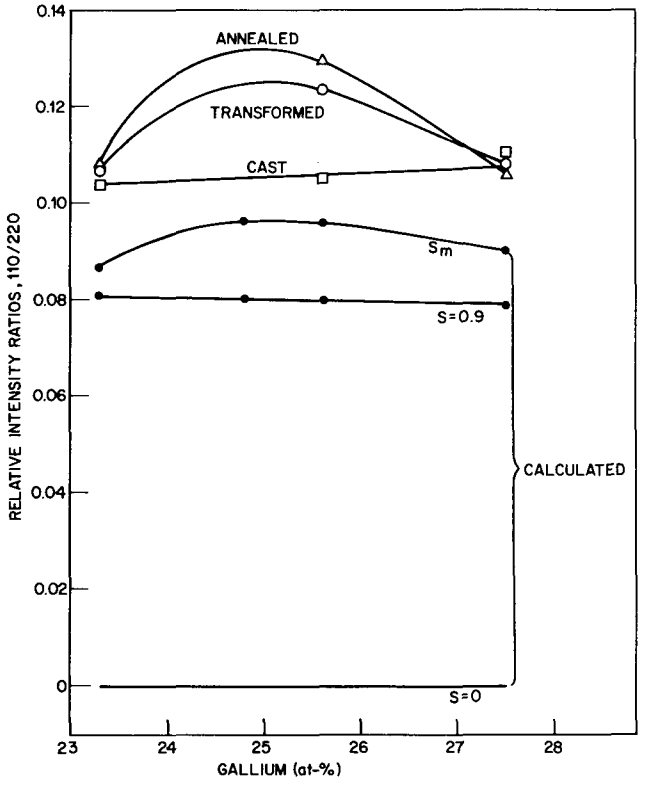

Fig. 15—Integrated x-ray intensity ratio (110)/(200) as a function of the composition of the β phase

behavior, and the experimental ratios are far from the completely disordered condition (S = 0). The curve for the calculated 110/200 intensity ratios for maximum order (S_m) shows an upward convexity, and that for partial order (S = 0.9) shows a linear variation with composition. The experimental curve for the cast samples shows a linear variation, whereas the data for the transformed and annealed specimens show more curvature than the S_m data. The sharper convexity in the annealed specimen may indicate a higher degree of order than that in the transformed specimen.

The difference in absolute magnitudes of the calculated and experimental 110/200 intensity ratios is probably due to the uncertainty in the temperature-correction factor. For example the structure factor for 110 reflection is represented as (Table 5) $F_{110} = 2S(f_B - f_A)$, where $f_A = |f_V| \exp(-M_V)$ and $f_B = |f_{Ga}| \exp(-M_{Ga})$. Here f_V and f_{Ga} are the dispersion-corrected atomic-scattering factors for V and Ga atoms respectively, and $\exp(-M_V)$ and $\exp(-M_{Ga})$ are the temperature-correction factors modifying the atomic-scattering factors for thermal vibrations. Again $M_V = B_V(\sin^2\theta/\lambda^2)$ and $M_{Ga} = B_{Ga}(\sin^2\theta/\lambda^2)$, where B_V and B_{Ga} are respectively the Debye parameters for V and Ga, θ is the Bragg angle, and λ is the x-ray wavelength. These Debye parameters for V and Ga atoms in V_3Ga are not accurately known but can be estimated from the reported Debye temperature (302 K) for V_3Ga [6]. The Debye parameters estimated in our calculation are the same for both V and Ga atoms, and this leads to the same temperature-correction factor for both V and Ga atoms in V_3Ga. In our calculations the same temperature-correction factor for both V and Ga atoms in V_3Ga has been used. However the coordination numbers and bonding of V and Ga atoms are different in V_3Ga; therefore the true Debye parameters will most likely be different. We have preliminary experimental evidence [18] that the Debye temperature of V in V_3Ga is 385 K as compared to 302 K, the Debye temperature of the V_3Ga compound. The higher Debye temperature for V atoms decreases the differences between experimental and calculated intensity ratios.

Our experimental intensity ratios are in better agreement with the intensity ratios reported by Koch [7] than those published by Nembach [19] or Levinstein [10]. However we agree with both Koch and Levinstein that the degree of order is high in all samples, even in the as-cast state. Metallographic evidence clearly shows however that the cast V_3Ga (Figs. 7 through 9) and the cast specimens annealed at low temperature without the high-temperature treatment (Figs. 10 and 11) are inhomogeneous. Thus we agree with Koch that powder x-ray diffraction is too insensitive to measure subtle changes in long-range order. In other words, localized regions in inhomogeneous specimens may be highly ordered, and the degree of order changes with composition from region to region. Powder x-ray diffraction cannot differentiate this change of order from one microscopic region to another; thus the value obtained is an average value of the inhomogeneous specimen.

Superconducting Transition Temperature

All reports of the superconducting transition temperature at zero field (T_0) of the A15 phase in the V-Ga system agree that T_0 is highly dependent on composition. Van Vucht et al. [1] report the maximum in T_0 for this phase to be 14.3 K at the stoichiometric composition. Efimov et al. [5] report a maximum of 15.8 K at 26 at-% Ga. Moreover, according to van Vucht et al., T_0 drops rapidly as the composition deviates

from stoichiometry, but the data of Efimov et al. show T_0 decreasing slowly to 13.5 K as the Ga content increases to 31 at-%. These conflicting observations prompted a study of superconducting transition temperatures in the A15 phase of the V-Ga system.

Transition temperatures were determined from the midpoint of the relative susceptibility change. As in many A15 compounds at fields below a few hundred oersteds, the plot of $H_{c2}(T)$ versus T_c deviates from linearity, and a measured zero-field transition (T_0) can be as much as several tenths of a Kelvin higher than the value obtained by extrapolating the H_{c2}-versus-T_c data to $H_{c2} = 0$ (Fig. 16). When the extrapolated value of T_0 is used, the parabolic relation

$$H_{c2}(T) = H_{c2}(0)\,[1 - (T/T_0)^2] \qquad (1)$$

(expected to hold near T_0) is self consistent. Here $H_{c2}(T)$ is the temperature-dependent magnetic field and $H_{c2}(0)$ is that field at 0 K. However a different value of $H_{c2}(0)$ is obtained for each measured value of $H_{c2}(T)$ and T_c when the measured T_0 is used. Thus our T_0 data are midpoint critical temperatures extrapolated to zero applied magnetic field.

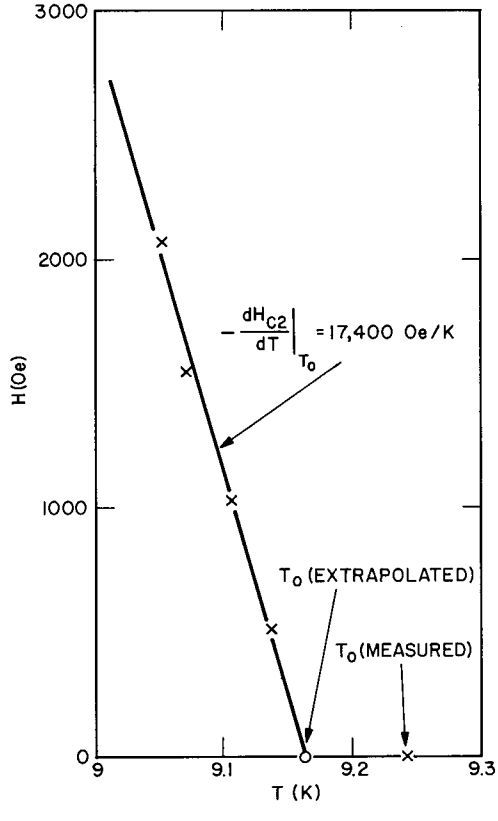

Fig. 16—Transition temperatures measured in magnetic fields, illustrating the difference in the measured and extrapolated T_0 values and the determination of the initial slope for an annealed V-20.5Ga specimen

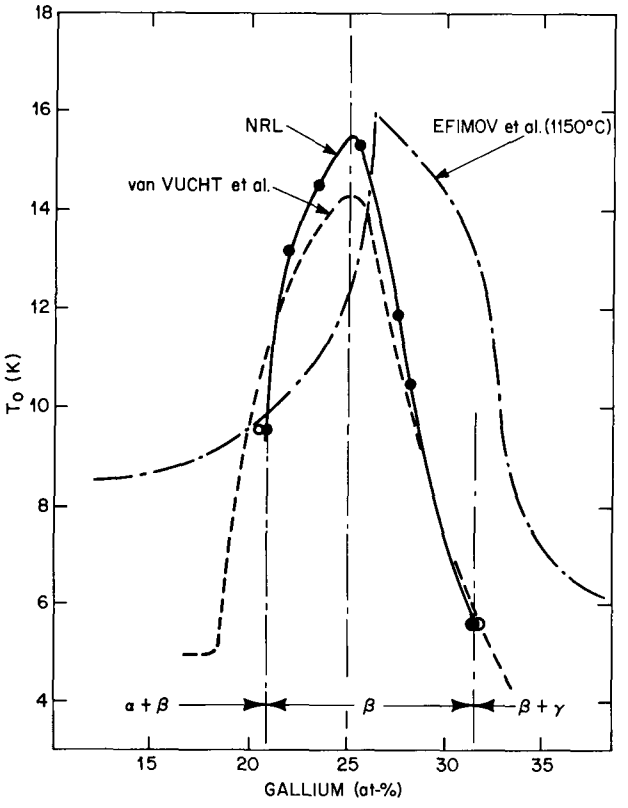

Fig. 17—The superconducting transition temperatures T_0 of transformed samples of V-Ga as a function of composition. Results reported by van Vucht et al. [1] and Efimov et al. [5] are presented for comparison.

The results of van Vucht et al. [1] and Efimov et al. [5] are compared with our transformed-sample data in Fig. 17. Our data are similar to those reported by van Vucht et al.; that is, T_0 drops rapidly as the composition deviates to either side of the stoichiometric composition V_3Ga. The somewhat slower drop in T_0 as the Ga content is decreased, compared to the more rapid drop as Ga is increased, is ascribed to the preservation of the integrity of the linear chains of V atoms in the A15 structure. We believe that the relatively higher T_0 values in our specimens near the stoichiometric composition compared with those reported by van Vucht et al. [1] are a consequence of the bcc α-phase homogenization and the use of higher purity (99.95%) V. Our results are also in agreement with Wernick et al. [20] and Junod et al. [6] but disagree considerably with those published by Efimov et al. [5].

The effect of heat treatment on transition temperatures is shown in Fig. 18 in the plot of T_0 as a function of Ga concentration. Since we know from our long-range-order study that the annealed specimens have a higher degree of order than do the transformed samples, the slightly lower T_0 values (by about 0.5 K) of the annealed specimens conflicts with the concept that T_0 increases as the long-range order improves. Either the change in electron-phonon interaction due to the nonuniform Ga distribution in the

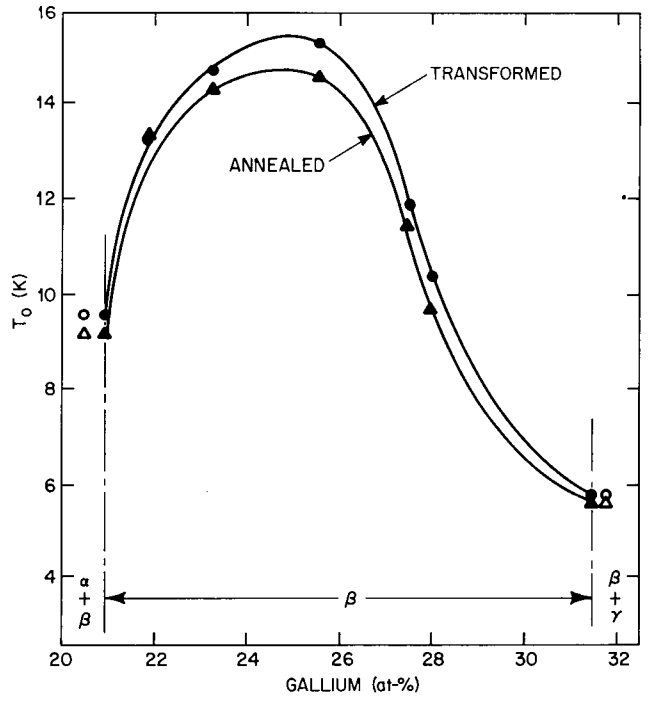

Fig. 18—The changes in superconducting transition temperatures T_0 with heat treatment of V-Ga

transformed specimens or the presence of {111} stacking faults and the disruption of the V chains [21] in the annealed specimens may be responsible for this anomaly.

The profile of normal-to-superconducting-state transitions as shown in Fig. 19 is sharpest at stoichiometry and becomes extended as the composition deviates to either side of stoichiometry. Both the transformed and annealed specimens show similar compositional dependences, with the annealed samples displaying slightly narrower transitions.

The samples used for the measurement of T_0 had rather irregular shapes and weighed between 1/4 and 1/2 g. Each sample was initially a 1.3-cm-long rod with approximately a rectangular cross section and was cut as a diametrical section from the 1.3-cm-diameter casting. However the brittleness of the compound and the existing cracks in the material made the specimens far from regular in shape, for portions of the surfaces were fracture surfaces. Since the transformed and the annealed specimens were from different but adjacent portions of the cast rod, there may be some small variation in the chemical composition of the pairs of specimens. But this composition variation is less than 0.5 at-% Ga according to lattice-parameter measurements.

Although the microstructure of the specimens gave no indication of a radial chemical gradient in the heat-treated specimens, the superconductivity transitions clearly revealed this in three samples of different compositions. An example is shown in Fig. 20 for an annealed V-25.6Ga sample in an applied field of 1000 Oe. The ends of this sample were surfaces that had been in contact with the mold wall, and the superconducting-to-normal

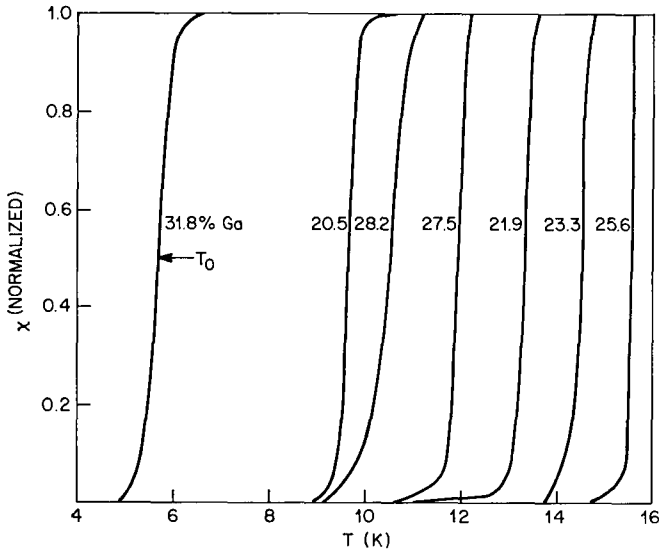

Fig. 19—Profiles of normal-to-superconducting-state transitions across the β-phase field of V-Ga

transition revealed two distinct transitions. When the surfaces that had contacted the wall were cut away, the lower temperature transition was eliminated.

The presence of multiple transitions or breaks in the normal-to-superconducting transitions indicate composition variations in the specimens. These composition variations are caused by the segregation occurring during solidification. The solidification segregation in cast ingots of V-Ga specimens is due to the large separation between liquidus and solidus lines as indicated in the existing phase diagram (Fig. 1). The surface of the casting will be lean in Ga, and the core will be rich in Ga. Extensive diffusion of Ga is required to eliminate this segregation. Failing this, the specimen will show two or more transitions or breaks in the normal-to-superconducting transition. In this system the microstructure is not sensitive to small changes in composition; thus metallographic studies will not detect this segregation. Although lattice-parameter measurements should be capable of revealing such segregation, the sampling must be done with care. The superconducting transition provides the clearest evidence of the solidification segregation.

Recently Koch [7] showed that annealing cast V_3Ga specimens for long intervals at 650 to 700°C caused an increase in T_0 by 1 to 1.6 K and that T_0 showed a tendency to decrease if the annealing temperature exceeded 700°C. Our metallographic observations show that such low-temperature anneals do not homogenize the cast structure even if the annealing period is extended to 3 weeks (Fig. 10). Also, our data show comparable T_0 values for materials homogenized at high temperature and rapidly cooled (transformed) or subsequently annealed at 1150°C. After reading Koch's results, we reannealed the annealed specimens of V-25.6Ga and V-27.5Ga at 700°C for 2 weeks. The T_0 of V-25.6Ga recovered from the value of the annealed specimen to 15.23 K, which is near the transformed value. The T_0 of the V-27.5Ga was unchanged: 11.44 K as annealed and 11.45 K after the additional 700°C anneal. Thus these characteristic T_0 values were retained after a prolonged 700°C anneal.

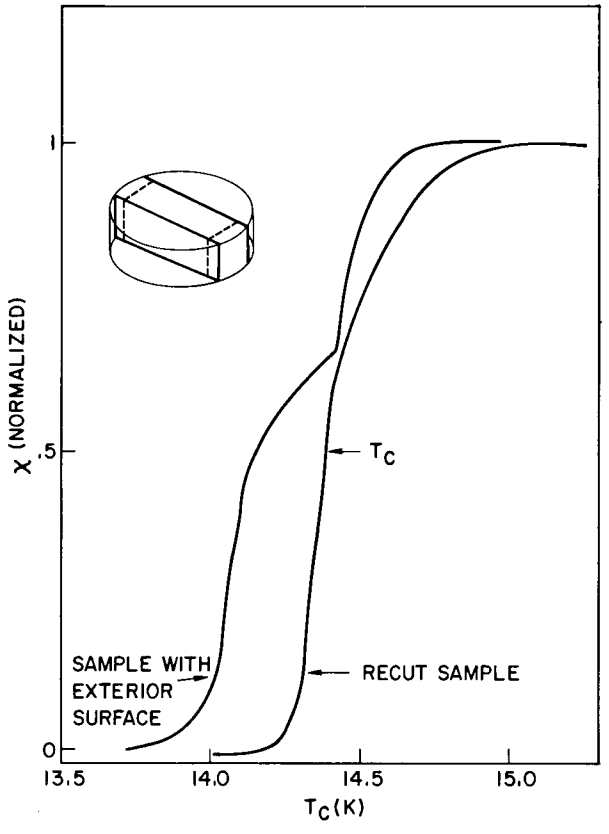

Fig. 20—Normal-to-superconducting transitions in the β phase of annealed V-25.6Ga with and without radial segregation. The presence of a step in the plot of susceptibility χ against temperature indicates the specimen inhomogeneity

Superconducting Parameters

In addition to determining T_0 we measured the initial slope of the critical-magnetic-field curves $(-dH_{c2}/dT)_{T_0}$ for each of the specimens. These measurements permit the evaluation of several theoretical zero-temperature magnetic-field predictions from the following equations. The Ginzburg-Landau upper critical magnetic field at zero temperature [22] is

$$H^*_{c2}(0) = 0.693T_0(-dH_{c2}/dT)_{T_0} \tag{2}$$

when magnetic fields (H) are given in oersteds and temperatures are in kelvins. The zero-temperature upper critical field, wherein paramagnetic effects have been included, can be calculated according to Maki [23] and Hechler et al. [24] as

$$H^{**}_{c2}(0) = H^*_{c2}(0)(1 + \alpha^2)^{-1/2}, \tag{3}$$

where

$$\alpha = 5.33 \times 10^{-5}(-dH_{c2}/dT)_{T_0}. \tag{4}$$

The paramagnetic upper critical field limit of Clogston [25] is given by

$$H_{c2}^{P}(0) = 18.4T_0. \tag{5}$$

The measured values of T_0 and $(-dH_{c2}/dT)_{T_0}$ and the calculated values of these upper critical fields are shown in Table 8.

Comparable data from previous studies of V_3Ga are shown in Table 9. The initial-slope values of Wernick et al. [20] for compositions of 23 to 29 at-% Ga are approximately twice ours, whereas their T_0 values are in reasonable accord with ours. The other reports of individual "V_3Ga" specimens give values of temperature and slope that are more in agreement with our results. Montgomery and Wizgall [26] measured several types of samples including diffusion layers, Kunzler wires, and sintered samples. The "sintered bulk as cast" samples, measured resistively, yielded the values 14.17 K and −39.4 kOe/K shown in the table. From the brief descriptions of specimen preparation and some rather confusing descriptions used in characterizing the specimens, we must assume that these samples were probably inhomogeneous.

To calculate other theoretically predicted parameters, it is necessary to know either the coefficient of the electronic component of the specific heat γ or the normal-state resistivity ρ_n at the superconducting transition temperature. Resistivity measurements were attempted, but because our samples were small and irregular, such measurements were inconclusive. We have used the results of the specific-heat measurements of Junod et al. [6] in our calculations. Because the heat treatment of Junod's samples differs from ours, we will not assign the γ values to either of our sample states explicitly. For these calculations we will use a single value of γ for each composition for both transformed and annealed samples, thereby tacitly assuming only a small change in γ with thermal treatment. We can calculate the Maki parameter α from the initial slope of the critical-magnetic-field curves via Eq. 4 and use the results of Junod et al. for γ to calculate ρ_n, since [23,24]

$$\rho_n = \alpha/2.35\gamma \tag{6a}$$

or

$$\rho_n = \frac{5.33 \times 10^{-5}(-dH_{c2}/dT)_{T_0}}{2.35\gamma}. \tag{6b}$$

Here ρ_n is in Ω-cm and γ is in ergs/cm^3-K^2. Using the formula of Hake [22] and Goodman [29], one can obtain the total Ginsburg-Landau parameter

$$\kappa_G = \kappa_0 + \kappa_l, \tag{7}$$

where the intrinsic Ginsburg-Landau parameter is

$$\kappa_0 = 1.61 \times 10^{24}\gamma^{3/2}T_0[n^{4/3}(S/S_f)^2]^{-1}$$

and the extrinsic Ginsburg-Landau parameter is

Table 8
Measured Superconductivity Parameters of the A15 Phase in the V-Ga System

Composition (at-%)	Thermal Treatment (temperature in degrees Celsius and, in parentheses, time in hours)*	a_0 (Å)	T_0 (K)	$\left\|\frac{-dH_{C2}}{dT}\right\|_{T_0}$ (kOe/K)	$H_{C2}(0)$ (kOe)	$H^{*}_{C2}(0)$ (kOe)	$H^{**}_{C2}(0)$ (kOe)	$H_{C2}(0)^{P}$ (kOe)	Maki Parameter α
V-20.5Ga†	1400(4)	—	9.53	15.1	73.5	99.7	77.7	175.4	0.805
	1400(4); 1225(6); 1150(7)	4.8140	9.16	17.4	77.4	110.5	81.0	168.5	0.927
V-21.9Ga	1400(4)	—	13.20	20.5	142.1	187.3	126.4	242.6	1.093
	1400(4); 1100(5)	4.8156	13.25	22.0	173.7	202.0	131.0	243.7	1.173
V-23.3Ga	1400(4)	—	14.65	22.2	170.9	225.4	145.5	269.5	1.183
	1400(4); 1150(7)	4.8168	14.28	23.8	168.2	235.5	145.8	262.8	1.269
V-25.6Ga	1400(4)	—	15.26	22.0	167.6	232.7	151.0	280.8	1.173
	1400(4); 1150(7)	4.8178	14.56	26.0	189.0	262.3	153.5	267.9	1.386
	1400(4);1150(7);700(335)	—	15.23	25.0	188.4	264.0	158.4	280.3	1.333
V-27.5Ga	1400(4)	—	11.88	11.0	68.0	90.5	78.1	218.5	0.586
	1400(4); 1150(7)	4.8218	11.44	28.3	158.6	224.4	124.0	210.5	1.508
	1400(4);1150(7);700(335)	—	11.46	35.5	275.6	282.0	131.8	210.9	1.892
V-28.2Ga	1400(6)	—	10.33	4.9	26.1	35.1	34.0	190.1	0.261
	1400(6); 1150(5)	4.8243	9.69	29.1	173.7	195.4	105.9	178.3	1.551
V-31.8Ga†	1275(5)	—	5.61	11.1	35.2	43.2	37.1	103.2	0.592
	1275(5); 990(7)	4.8325	5.50	17.0	46.9	64.8	29.5	101.2	0.906

*Temperatures at the left side of the column are homogenization temperatures prior to rapid cooling to yield transformed specimens (α-to-β transformation). Additional temperatures are annealing and reannealing temperatures within the β-phase field.
†Two-phase sample.

Table 9
Literature Values of the Critical Temperature and Initial Slope of the A15 Phase in the V-Ga System

Authors	T_0 (K)	$\left.\frac{-dH_{C2}}{dT}\right\|_{T_0}$ (kOe/K)	V_3Ga Specimen
Wernick et al. [20]	14.5	50	Ingot composition from 23 to 33 at-% Ga. Values shown are for V-25.3Ga.
Heckler et al. [24]	14.83	34	Cu-plated and annealed for 50 hr at 700°C.
Otto et al. [27]	14.1	39	Sintered rod.
Decker and Laquer [28]	14.2	43.2	"As cast hollow spark-cut cylinder."
Montgomery and Wizgall [26]	14.17	39.4	"Sintered bulk as cast."

$$\kappa_\ell = 7500\,\rho_n\gamma^{1/2}.$$

Hake [30] estimated S/S_f as 0.6 and n as 3.22×10^{23} per cm^{-3} for V_3Ga.

One can also determine the electron mean-free path ℓ, the coherence distance $\xi_{0_{BCS}}$, and the density of states at the Fermi surface for one spin direction N, from the following relations [22]:

$$\ell = 1.27 \times 10^4\left[\rho_n n^{2/3}\left(\frac{S}{S_f}\right)\right]^{-1}, \tag{8}$$

$$\xi_{0_{BCS}} = 7.93 \times 10^{-17} n^{2/3}\left(\frac{S}{S_f}\right)(\gamma T_0)^{-1}, \tag{9}$$

and

$$N(0) = 8.0 \times 10^{30}\gamma. \tag{10}$$

According to the BCS theory [31]

$$T_0 = 0.855\Theta_D \exp -\left[\frac{1}{N(0)V}\right], \tag{11}$$

where Θ_D is the Debye temperature, N(0) is the density of electronic states at the Fermi level, and V is the pairing potential arising from the electron-phonon interaction. For strong coupling superconductors, McMillan [32] has derived the expression

$$T_0 = \frac{\Theta_D}{1.45} \exp\left[-\frac{1.04(1+\lambda)}{\lambda - \mu^*(1+0.62\lambda)}\right], \tag{12}$$

where μ^* is the Coulomb coupling constant and λ is the electron-phonon coupling constant. McMillan takes 0.13 as the value of μ^* for all transition metals and their alloys, but a better value for V-based A15 material is probably 0.19 [33]. Thus, knowing T_0 and Θ_D, one can solve for λ and in turn the band-structure density of states N_{bs} (0) given [32] as

$$N_{bs}(0) = 3\gamma[2\pi^2 k_B^2(1+\lambda)]^{-1} = N_\gamma(0)(1+\lambda)^{-1}, \tag{13}$$

where k_B is Boltzmann's constant.

Calculated values of these parameters are listed in Table 10 for the samples that had compositions approximately equal to those reported by Junod et al. [6]. In this table γ and Θ_D values are from that paper [6], ρ_n is the normal-state resistivity evaluated near 4.2 K, and the various values of κ relate to intrinsic sample characteristics which in the case at hand indicate the degree of type-II character for these samples. The remainder of the parameters are those already discussed.

The literature contains sparse reporting of measured γ and ρ_n values. Knapp and Jones [34] report 14.5 K for T_0 and 5.94×10^3 ergs/cm^{3}K^2 for γ. Morin et al. [35] report a γ value of 30.3×10^3 erg/cm^{3}K^2 for a V_3Ga sample. Using this number with their [35] values of 14.66 K for T_0 and -40.2 kOe/K for the initial slope, one obtains from Eqs. 6 and 7 values for κ_0, κ_ℓ, and κ_G of 16, 39, and 55 respectively and a value of 30 $\mu\Omega$-cm for ρ_n. Usually, for compounds, κ_0 is at most a few percent of κ_ℓ and therefore only a few percent of κ_G. Another expression that can be used for the total Ginsburg-Landau parameter as given by Hake [22] is

$$\kappa_1(T_0) = (6.0\gamma^{1/2})^{-1}\left(\frac{-dH_{c2}}{dT}\right)_{T_0} \tag{14}$$

whereby $\kappa_1(T_0) = 38$. It would appear that κ_0 is large due to the value of γ, which for Morin et al. [35] is nearly 5 times larger than the value of γ determined by Junod et al. [6] and by Knapp and Jones [34]. However the ρ_n values correlate well with the value 37.4 $\mu\Omega$-cm determined by Sarachik et al. [36] and with the value 41 $\mu\Omega$-cm determined by Montgomery and Wizgall [26]. All three resistivity values are lower by a factor of approximately 2 than our calculated values.

The initial slopes of the critical-magnetic-field curves as a function of Ga concentration are shown in Fig. 21. As was the case in previous studies of both the V-Pt [37] and V-Ir [38] systems, the data of the annealed samples conform to a smoother, less widely varying function of composition than do the data of the transformed samples. However the α-to-β solid-state transformation became sluggish above the 28-at-%-Ga composition, which is just the composition that $(-dH_{c2}/dT)_{T_0}$ achieves its relative maximum and minimum values for the annealed and transformed cases respectively. Perhaps the behavior of this parameter is correlated to an as-yet-undetermined structural feature of the metallurgical system.

Table 10
Calculated Parameters of the A15 Phase in the V-Ga System (values of γ and Θ_D are from Janod [6], values of N are from Eq. 10, values of N(0)V are from Eq. 11, and values of $N_{bs}(0)$ are from Eq. 13)

Composition (at-%)	γ erg cm^3K^2	Θ_D (K)	N (10^{34} erg^{-1} cm^{-3})	Thermal Treatment†	ρ_n (10^{-4} Ω-cm)	$\kappa_1(T_0)$	κ_G	κ_0	κ_ℓ	ℓ (10^{-7} cm)	$\xi_{0_{BCS}}$ (10^{-7} cm)	λ	N(0)V	$N_{bs}(0)$ (10^{34} states/ V atom
V-21.9Ga	3952	326	3.16	A	1.177	54.4	54.7	0.65	54	0.38	43.3	1.08	0.328	1.52
				A+B	1.263	58.3	58.7	0.65	58	0.35	43.1	1.08	0.328	1.52
V-25.6Ga	7215	302	5.77	A	0.692	43.2	44.9	1.90	43	0.65	20.3	1.21	0.337	2.61
				A+C	0.818	51.0	52.8	1.81	51	0.55	21.2	1.18	0.348	2.64
				A+C+D	0.786	49.1	50.7	1.90	49	0.57	20.3	1.21	0.353	2.61
V-27.5Ga	5002	310	4.00	A	0.483	25.9	25.9	0.87	25	0.94	37.3	1.05	0.322	1.94
				A+C	1.283	66.7	68.8	0.84	68	0.35	38.7	1.03	0.318	1.97
				A+C+D	1.610	83.7	71.8	0.84	71	0.28	38.6	1.04	0.318	1.96
V-31.8Ga*	1968	363	1.57	E	1.279	41.7	43.1	0.10	43	0.36	197.1	0.76	0.249	0.89
				E+F	1.959	63.7	63.1	0.10	63	0.24	201.1	0.76	0.248	0.89

*Two-phased sample.
†A = 1400° C for 4 hr, B = 1100° C for 5 hr, C = 1150° C for 7 hr, D = 700° C for 335 hr, E = 1275° C for 5 hr, and F = 990° C for 7 hr.

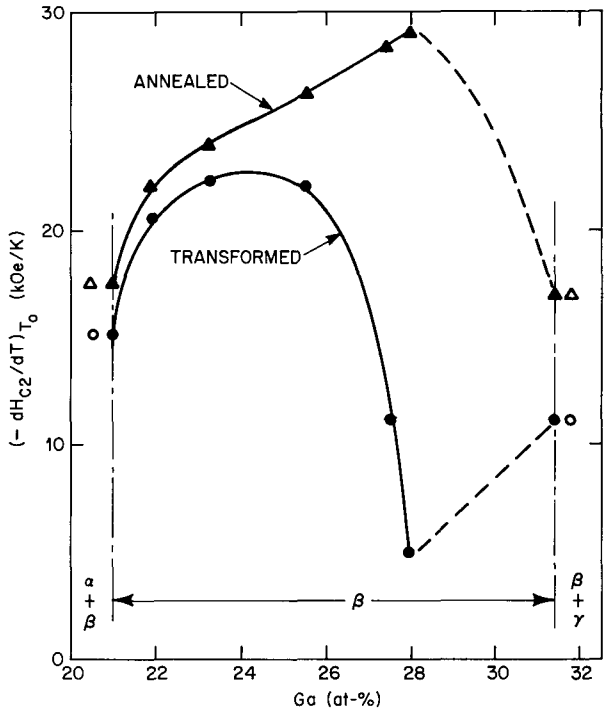

Fig. 21—The initial slopes of the critical-magnetic-field curves of the β phase of V-Ga as a function of Ga concentration and heat treatments

On the other hand, we see from Eq. 6b that $(-dH_{c2}/dT)_{T_0}$ is proportional to γ and from Eq. 10 and 13 that γ is in turn proportional to N(E), where N(E) is any of the forms of the electronic density of states given in Eqs. 10 and 13. A maximum in $(-dH_{c2}/dT)_{T_0}$ implies a maximum in the density of states if ρ_n is a slowly varying function of composition, and it would appear according to the rigid band model that, for the V-Ga system, the Fermi level is closest to the peak in the density of states at the 28-at-%-Ga composition. If this is the case, then measurements of the initial slopes of the critical-magnetic-field curves enable one to determine the composition for which the Fermi level is closest to the maximum in the density of states quite readily and simply for any superconducting material.

If the density of states per se was governing the superconducting properties, simple models relating T_0 and N(E) suggest that T_0 should maximize at 28 at-% Ga. That it does not suggests that another mechanism predominates, and the model most widely accepted for A15 materials is the linear-chain model developed by Labbé and Freidel [39]. Basically their model states that T_0 is intimately connected and directly proportional to the crystallographic long-range order of the system. We have already discussed the effects of long-range order brought about by the thermal processing of the alloys. However another facet to the long-range-order picture is that brought about by altering the chemical composition of the alloy, and this is the view to be considered now. On the Ga-deficient side of stoichiometry, the integrity of the linear chain is maintained. At stoichiometry there is exactly enough V to fill all of the linear chain sites and exactly enough Ga to fill all the bcc sites. With progression to the Ga-rich side of stoichiometry,

there is not sufficient V to fill all the chain sites; so the excess Ga atoms fill them, thereby breaking up the linear V chains.

The rationale behind the Labbé-Freidel model is the integrity of the linear chains. That being so, one would expect T_0 to be relatively independent of composition on the Ga-deficient side of stoichiometry, where the linear chains are full; but on the Ga-rich side of stoichiometry their model predicts a strong dependence of T_0 on composition, since the Ga atoms will be breaking up the chains. Thus the behavior witnessed in Fig. 17 for either the transformed or the annealed samples on the Ga-rich side of stoichiometry conforms with the Labbé-Friedel model. However the decrease in T_0 as the composition shifts from stoichiometry on the Ga-deficient side does not agree with this model. Possibly the presence of V atoms in sites intended for Ga is responsible for the breakdown of the linear chain model due to the fact that intrachain interactions are no longer negligible. The V-Pt system [37] is a nice example of the Labbé-Freidel model, wherein the B element was a transition metal. Perhaps the fact that Ga is a nontransition metal means that the V electrons at chain sites are at liberty to interact with electrons of V at bcc sites, whereas in the V-Pt case, electrons of bcc vanadium were prevented by the electrons of Pt from doing so.

SUMMARY

The results from these studies of the superconducting A15 phase of the V-Ga system can be summarized as follows:

- Within the range of compositions examined the phase equilibria of the V-Ga system determined by van Vucht [1] appear to be correct. The present results indicate a narrower composition range for the β phase and a displacement of the $\alpha + \beta$ field to higher Ga content.

- The arc-melting and casting procedures produced cylindrical rods of uniform microstructure for these studies. As a consequence of the broad liquid-plus-α-phase field, the castings displayed dendritic segregation and a large-scale radial Ga gradient. This gradient evident in high-Ga alloys by the retention of a metastable α phase at the core of the casting, was not evident in the microstructures of most of the alloys. However the superconducting-transition-temperature determinations proved to be a sensitive detector of this gradient. This gradient will be present for all arc-cast samples regardless of geometry, and we believe this is responsible for many of the inconsistent T_0 values reported in the literature.

- The dendritic segregation in the cast materials was made visible in metallographic sections by suitable etching procedures. Anneals of several hundred hours at 1100°C were ineffective in eradicating this segregation. However a brief heat treatment at temperatures in the α-phase field does homogenize the material. By rapidly cooling the specimen through the α-to-β transformation, segregation from the transformation occurs on a fine scale and such fine-scale segregation can be removed by a subsequent anneal within the β-phase field.

- Although the composition range of the β-phase is rather broad, the transformed microstructures and the annealed microstructures of all of the β-phase materials were

similar. Thus property measurements as a function of composition are from specimens of similar microstructure. Even microhardness values, previously reported to show a minimum near the V_3Ga composition, were nearly constant over the full composition range of the β-phase.

- The lattice parameter of the β phase increases with increasing Ga content. The present measurements define two lines intersecting near the V_3Ga composition. These data support the proposal that the compositional adjustment is a substitution of A and B atoms in A_3B; that is, Ga replaces excess V in B sites, causing a small expansion of the lattice as the Ga content is increased to the V_3Ga composition, and beyond the V_3Ga composition Ga replaces V in A sites and causes a large lattice expansion.

- Long-range-order studies showed that the β phase is highly ordered—even in the cast state. In these nonhomogeneous materials local order is probably high in all regions, but the measurement is an average of these zones of different compositions and hence of different maximum atomic order. The improvement in the long-range-order parameter with heat treatment reflects the increased homogeneity of the sample rather than an intrinsic change in order.

- Measurement of T_0 without accompanying critical-magnetic-field information can give T_0 values up to several tenths of a kelvin too high. The same phenomenon has been witnessed in other A15 systems, but no explanation has been suggested to date.

- T_0 is higher for the transformed samples than for the annealed samples. The reason for this is not known either, but it cannot be attributed to surface effects resulting from the anneal, because all specimens for T_0 measurements were cut from the interior of larger heat-treated samples.

- We do not understand the reason for the dissimilarity of the appearance of the initial-slope curve for the annealed as opposed to the transformed samples as a function of composition. Analogous discrepancies have been seen in the V-Pt and V-Ir systems.

- Analysis of the initial slope of the critical-magnetic-field-vs-composition plot and of the transition-temperature-vs-composition plot suggest that on the Ga-rich side of stoichiometry the Labbé-Friedel [39] linear-chain model holds but on the V-rich side the density-of-states model seems more valid. Far-infrared optical-spectroscopy studies may someday resolve this dilemma. Another avenue of resolution would be specific-heat measurements on a series of V-Ga alloys with small composition increments ($\approx$ 0.5%) in the range 25 to 28 at-% Ga. The same sample should be measured in the transformed state and then remeasured in the annealed state. If one accepts the proportionality of the density of electronic states to the magnitude of the initial slope of the critical magnetic field curve via Eq. 6b, then superconductivity measurements enable one to determine the composition for which the Fermi level most nearly approaches the peak in the density of states for a given alloy system. There is some concern that the critical-field curves do not follow theoretical predictions, so that the relationship between γ and $(-dH_{c2}/dT)_{T_0}$ may not be directly applicable.

ACKNOWLEDGMENTS

We thank R. A. Meussner for the critical reading of the manuscript, R. W. Scott and W. E. King, Jr. for the help in constructing the induction annealing furnace, and C. R. Forsht for the help in melting and casting the specimens.

REFERENCES

1. J.H.N. van Vucht, H.A.C.M. Bruning, H.C. Donkersloot, and A.H. Gomes de Mesquita, "The System Vanadium-Gallium," Philips Res. Repts. 19, 407-421 (1964).
2. D.G. Howe and L.S. Weinman, Proc. Fifth Intl. Cryo. Eng. Conf., Kyoto, Japan, May 7-10, 1974. "Superconducting Properties of V_3Ga in the V-Ga/Cu-Ga Composite System," p. 326.
3. International Tables for X-Ray Crystallography, Vol. 3, 1968, Table 3.3.2B, p. 214.
4. E. Maxwell, "Mutual Inductance Bridge for ac Susceptibility Measurements at Low-Frequencies," *Rev. Sci. Instr.* 36, 553 (1965).
5. Yu.V. Efimov, V.V. Baron, and E.M. Savitskii, "Structure and Superconducting Properties of V-Ga Alloys," pp. 147-153 in *Physics and Metallurgy of Superconductors*, edited by E.M. Savitskii and V.V. Baron, New York Consultants Bureau, 1970.
6. A. Junod, J.L. Staudenmann, J. Muller, and P. Spitzli, "Superconductivity, Density-of-States Models, and Specific Heat of A15 Type Compounds V-Ga and V-Si," *J. Low Temp. Phys.* 5 (No. 1), 25-43 (1971).
7. C.C. Koch, "On Annealing, Long Range Order and Superconducting Transition Temperature in the V_3Ga A15 Compound," *J. Phys. Chem. Solids*, 34(No. 8), 1445-1448 (1973).
8. H. von Philipsborn and F. Laves, "The Influence of Impurities on the Formation of the Cu_3Au-Type Structure from the Cr_3Si-Type Structure," *Acta Cryst.* 17, 213-214 (1964).
9. B.T. Matthias, "Superconductivity and Hardness," *Phys. Letters* 25A, 226-227 (1967).
10. H.J. Levinstein, J.H. Wernick, and C.D. Capio, "Some Properties of the A15 Phase in the V-Ga System," *J. Phys. Chem. Solids* 26, 1111-1117 (1965).
11. E.M. Savitskii, P.I. Kripyakevich, V.V. Baron, and Yu.V. Efimov, "Phase Diagram of the Vanadium-Gallium System," *Inorg. Mat.* 3, 35-42 (1967).
12. S.M. Kuznetsova and G.S. Zhdanov, "Atomic Structure and Superconductivity of V_3Ga," *Soviet Phys. Crystallogr.* 16, 1077-1080 (1972).
13. R.D. Blaugher, R.A. Hein, J.E. Cox, and R.M. Waterstrat, "Atomic Ordering and Superconductivity in A15 Compounds," *J. Low Temp. Phys.* 1, 539-561 (1969).
14. R.A. Hein, J.E. Cox, R.D. Blaugher, R.M. Waterstrat, and E.C. van Reuth, "Low-Temperature Annealing Effects upon the Superconducting Properties of V_3Au," *Physica*, 55, 523-533 (1971).
15. B.E. Warren, *X-ray Diffraction*, Reading, Mass., Addison-Wesley, 1969, p. 208.

16. E.C. van Reuth and R.M. Waterstrat, "Atomic Ordering in Binary A15-Type Phases," *Acta Cryst.* **B24**, 186–196 (1968).

17. Table 3.3.1A on p. 204 of Ref. 3.

18. C.L. Vold, private communication to be published.

19. E. Nembach, "Defect Structure and Critical Current Density in the High Field Superconductors V_3Ga, $(VZr)_3Ga$, and $(VHf)_3Ga$," *Z. Metallkde* **61**, 734–742 (1970).

20. J.H. Wernick, F.J. Morin, F.S.L. Hsu, D. Dorsi, J.P. Maita, and J.E. Kunzler, "Evidence for a Critical Magnetic Field in excess of 500 Kilogauss in the superconducting V-Ga system, in High Magnetic Fields," ed. by H. Kolm, B. Lax, F. Bitter, and R. Mills, M.I.T. Press, Cambridge, Mass., and New York, 1962, pp. 609–614.

21. U. Essmann and G. Zerweck, "$1/2 <111>$ Stacking Faults in A15 (β - W) Superconductors," *Phys. Stat. Sol.* (b)**57**, 611–616 (1973).

22. R.R. Hake, "Paramagnetic Superconductivity in Extreme Type-II Superconductors," *Phys. Rev.* **158**, 356 (1967).

23. K. Maki, "The Magnetic Properties of Superconducting Alloys, II," *Phys.* **1**, 127 (1964); "Effect of Pauli Paramagnetism on Magnetic Properties of High Field Superconductors," *Phys. Rev.* **148**, 362 (1966).

24. K. Hechler, G. Horn, G. Otto, and E. Saur, "Measurements of Critical Data for Some Type II Superconductors and Comparison with Theory," *J. Low Temp. Phys.*, **1**, 29 (1969).

25. A.M. Clogston, "Upper Limit for the Critical Field in Hard Superconductors," *Phys. Rev. Letters* **9**, 266 (1962).

26. D.B. Montgomery and H. Wizgall, "Measurement of the Upper Critical Field of Vanadium-Gallium Alloys," *Phys. Letters* **22**, 48 (1966).

27. G. Otto, E. Saur, and H. Wizgall, "Critical Data of Some A15 Type Superconductors in Transverse Fields up to 230 k0e," *J. Low Temp. Phys.* **1**, 19–28 (1969).

28. R.L. Decker and H.L. Laquer, "Magnetization Studies on Superconducting Vanadium-Gallium," *J. Appl. Phys.* **40**, 2817 (1969).

29. B.B. Goodman, "The Magnetic Behavior of Superconductors of Negative Surface Energy," *IBM J. Res. Development* **6**, 63 (1962).

30. R.R. Hake, "Upper-Critical-Field Limits for Bulk Type-II Superconductors," *Appl. Phys. Letters* **10**, 189 (1967).

31. J. Bardeen, L.N. Cooper, and J.R. Schrieffer, "Theory of Superconductivity," *Phys. Rev.* **108**, 1175 (1957).

32. W.L. McMillan, "Transition Temperature of Strong Coupled Superconductors," *Phys. Rev.* **167**, 331 (1968).

33. K.H. Bennemann and J.W. Garland, "Theory for Superconductivity in d-Band Metals," pp. 103–137 in *Superconductivity in d- and f-Band Metals*, edited by D.H. Douglass, American Institute of Physics, New York, 1972.

34. G.S. Knapp and R.W. Jones, "The Electron-Phonon Enhancement Factor and the Bare Density of V_3Ga," *Bull. Am. Phys. Soc.* **18**, 327 (1973).

35. F.J. Morin, J.P. Maita, H.J. Williams, R.C. Sherwood, J.H. Wernick, and J.E. Kunzler, "Heat Capacity Evidence for a Large Degree of Superconductivity in V_3Ga in High Magnetic Fields," *Phys. Rev. Letters* 8, 275 (1962).

36. M.P. Sarachik, G.E. Smith, and J.H. Wernick, "The Thermoelectric Power of V_3X Compounds," *Can. J. Phys.* 41, 1542 (1963).

37. J.E. Cox, R.A. Hein, and R.M. Waterstrat, "Superconducting Properties of A15 Phase V-Pt Alloys," p. 333 in Proc. 12th Int'l Conf. on Low-Temp. Phys., E. Kanda, editor, (1971).

38. J.E. Cox, J.L. Bostock, and R.M. Waterstrat, "Superconducting Properties of A15 Phase V-Ir Alloys," p. 480 in Proc. 13th Int'l Conf. on Low-Temp. Phys., W.J. O'Sullivan, K.D. Timmerhaus, and E.F. Hammel, editors Vol. 3, New York, Plenum, (1974).

39. J. Labbé and J. Freidel, "Instabilité Électronique et Changement de Phase Cristalline des Composés du Type V_3Si a Base Temperature," *J. Physique* 27, 153, 303, 708 (1966).